Experimental Determination of Electron Inelastic Mean Free Paths in 13 Elemental Solids in the 50 eV to 5000 eV Energy Range by Elastic-Peak Electron Spectroscopy

S. Tanuma[1]*, T. Shiratori[1,2]**, T. Kimura[1], K. Goto[3], S. Ichimura[4], and C. J. Powell[5]

[1]National Institute for Materials Science, 1-2-1 Sengen, Tsukuba, Ibaraki 305-0047, Japan

[2] Utsunomiya University, 7-1-2 Youtou, Utsunomiya, Tochigi 321-8585, Japan

[3]Nagoya Institute of Technology, Gokiso-chou, Showa-ku, Nagoya 466-8555, Japan

[4]National Institute of Advanced Industrial Science and Technology, 1-1-4 Umezono, Tsukuba, Ibaraki 305-8568, Japan

[5]National Institute of Standards and Technology, Gaithersburg, MD 20899-8370, USA

We have determined electron inelastic mean free paths (IMFPs) in C (graphite), Si, Cr, Fe, Cu, Zn, Ga, Mo, Ag, Ta, W, Pt and Au by elastic-peak electron spectroscopy (EPES) using Ni as a reference material for electron energies between 50 eV and 5000 eV. These IMFPs could be fitted by the simple Bethe equation for inelastic electron scattering in matter for energies from 100 eV to 5000 eV. The average root-mean-square (RMS) deviation in these fits was 9 %. The IMFPs for Si, Cr, Fe, Cu, Ag, Ta, W, Pt and Au were in excellent agreement with the corresponding values calculated from optical data for energies between 100 eV and 5000 eV. While the RMS differences for graphite and Mo in these comparisons were large (27 % and 17 %, respectively), the average RMS difference for the eleven elements was 11 %. Similar comparisons were made between our IMFPs and values obtained from the TPP-2M predictive equation for energies between 100 eV and 5000 eV, and an average RMS difference for the thirteen solids was 10.7 %; in these comparisons, the RMS differences for Ta and W were relatively large (26 % for each). A correction for surface-electronic excitations was calculated from a formula of Werner *et al*.; except for Si and Ga, the average correction was 5 % for energies between 150 eV and 5000 eV. The satisfactory consistency between the IMFPs from our EPES experiments and the corresponding IMFPs computed from optical data indicates that the uncertainty of these IMFPs is about 11 % for electron energies between 100 eV and 5000 eV. Similar comparisons with IMFPs from the EPES experiments of Werner *et al*. showed a consistency of 8 % for energies

between 200 eV and 5000 eV.

KEYWORDS: electron inelastic mean free paths; experimental determination; elastic-peak electron spectroscopy; Monte Carlo simulation

*Correspondence to: S. Tanuma, National Institute for Materials Science (NIMS), 1-2-1 Sengen, Tukuba, Ibaraki 305-0047, Japan

E-mail: Tanuma.Shigeo@nims.go.jp

** Present address: KOA corporation, 14016 Naka-Minowa, Minowa, Nagano 399-4697, Japan

INTRODUCTION

The electron inelastic mean free path (IMFP) is an important parameter in simulations of electron transport in solids and in quantitative surface analyses by Auger-electron spectroscopy (AES) and X-ray photoelectron spectroscopy (XPS). Values of IMFPs have been determined from calculations based on experimental optical data[1] because reliable experimental determinations of the IMFP can be difficult.[2] Tanuma *et al*.[3-10] have calculated IMFPs for over 70 materials from their optical energy-loss functions with the Penn algorithm[1] for 50 eV to 2000 eV electrons and shown the IMFP dependences on material parameters and electron energy. More recently, they have extended the energy range of their IMFP calculations to 30 keV.[11]

The accuracy of IMFPs for a given material depends on the accuracy of the particular energy-loss function on which the calculation is based. This uncertainty is typically less than 10 %, although it can be larger for some inorganic materials.[4,5] The other main source of inaccuracy is associated with approximations in the Penn algorithm. This uncertainty is believed to be about 10 % for free-electron-like materials and for energies larger than 200 eV.[6] The uncertainty of IMFPs for other materials and for energies less than 200 eV is expected to be larger.[6] Tanuma *et al*. also analyzed IMFPs for groups of elemental solids and organic compounds and derived an equation, designated TPP-2M, that could be used to estimate IMFPs for other materials.[7] The four parameters in TPP-2M could be empirically related to several material parameters (atomic or molecular weight, density, number of valence electrons per atom or molecule, and the band-gap energy for nonconductors). The TPP-2M equation was developed and originally tested for energies from 50 eV to 2 keV,[7] but its suitability for energies up to 30 keV appears promising.[11]

It is important to compare calculated IMFPs and those obtained from a predictive equation with experimental values in order to assess the consistency of the IMFP values. Elastic-peak electron spectroscopy (EPES) is a useful method for experimental determination of IMFPs.[2,12] In most EPES measurements, it has been convenient to compare elastic-backscattering coefficients from a material of interest with those of a suitable reference material. Alternatively, IMFPs can be determined from absolute measurements of elastic-backscattering coefficients. With the latter approach, it is necessary to make a correction for surface-electronic excitations; the method by which this correction should be applied, however, is still being investigated.

We report here IMFPs for thirteen elemental solids (C (graphite), Si, Cr, Fe, Cu, Zn, Ga, Mo, Ag, Ta, W, Pt and Au) derived from EPES experiments with 50 eV to 5000 eV electrons. Although absolute EPES intensities were measured, we obtained IMFPs from comparisons with elastic-peak intensities measured for a nickel reference material, one of the materials recommend by Powell and Jablonski.[2]

EXPERIMENTAL

Measurements of elastic-peak intensities

The energy dependencies of elastically backscattered primary electrons have been measured for graphite, Si, Cr, Fe, Cu, Zn, Ga, Mo, Ag, Ta, W, Pt, Au and Ni with a novel cylindrical mirror analyzer (CMA)[13] over the 1 eV to 5000 eV range. The polar acceptance angle of the CMA is 42.3 ± 6 degrees from the surface normal. All signals were measured by the electrometers (Keithley Model 642LN for the spectral current and Model 610A for the primary current).[a] These electrometers were calibrated with a picoampere source (Keithley Model 261)[a] that had been calibrated previously. It was thus unnecessary to correct measured spectra for dead-time effects, as required for electron-multiplier detectors. Each measurement of the height of the elastic peak was corrected, however, for the intensity-energy response function of the analyzer.

Except for graphite and silicon, all specimens were polycrystalline and were polished with diamond paste (0.5 μm particle size) and/or alumina paste (0.05 μm). The silicon (100) specimen was cut from a polished wafer, and then washed in ethyl alcohol and distilled water. Before the EPES measurements, the surfaces of all specimens except graphite were cleaned by sputtering with 250 eV argon ions to remove surface contamination. Occasionally, heavy contamination was encountered and was removed by sputtering with 500 eV to 600 eV argon ions; these surfaces were subsequently sputtered with 250 eV ions. The graphite surface was cleaned by peeling off a surface layer with tweezers.

---

[a] Commercial products are identified to specify the measurement procedure. Such identification does not imply recommendation or endorsement by the National Institute of Standards and Technology, nor does it imply that the products are necessarily the best available for the purpose.

Determination of IMFPs from elastic-peak intensity ratios

Monte Carlo (MC) simulations were performed to calculate the ratios of intensities, I^x / I^{Ni}, of elastically backscattered electrons for a sample *x* to those of the Ni reference, for our EPES configuration. These ratios can be described by the following equation:

$$\left(\frac{I^x}{I^{Ni}}\right) = \frac{f_S^x}{f_S^{Ni}} \frac{\int_0^\infty (d\eta/dS)^x / N_0^x \exp(-S/\lambda_x) dS}{\int_0^\infty (d\eta/dS)^{Ni} / N_0^{Ni} \exp(-S/\lambda_{Ni}) dS} \quad (1)$$

where, for sample and reference, f_s is a surface-electronic excitation (SEE) correction factor, $(d\eta/dS)$ is the path-length distribution of elastically backscattered electrons entering the CMA, λ is the IMFP, and N_0 is the number of trajectories in each MC simulation. The Ni IMFPs used in Eq. (1) were calculated from the Penn algorithm[1] and were cited in a previous paper.[14] If we assume that the ratio of surface-excitation correction factors, f_S^x / f_S^{Ni}, is unity, we can equate the intensity ratios from the EPES experiments with the calculated ratios from Eq. (1) and solve this equation to determine λ_x.

We calculated elastically backscattered electron intensities for 13 elemental solids over the 50 eV to 5000 eV energy range and for the Ni reference standard using Eq. (1). Since we need a very large number of random numbers in these calculations, the degree of randomness of these numbers is important. We used the Mersenne Twister, a pseudo-random number generator developed by Matsumoto *et al*.[15] that has a period of 2^{19937}-1.

Calculations of path-length distributions, $d\eta/dS$, require differential elastic-scattering cross sections for the relevant elements and for the energies of the EPES experiments. The differential cross section $d\sigma(E)/d\theta$ for elastic scattering of electrons of energy *E* by atoms is given by:[14,16]

$$\frac{d\sigma(E)}{d\theta} = |f(\theta)|^2 + |g(\theta)|^2 \quad (2)$$

where θ is the polar scattering angle, and $f(\theta)$ and $g(\theta)$ are the direct and spin-flip scattering amplitudes, respectively. These scattering amplitudes can be computed from relativistic Dirac theory using the partial-wave expansion method.[16] For simplicity, we used the analytical expression for the Thomas-Fermi-Dirac (TFD) potential for most of our calculations. In addition, we compared IMFPs for Ni, Si, Ag, and Au from the TFD potential with IMFPs obtained using differential cross sections computed from the more accurate[16] Dirac-Hartree-Fock potential.

In order to estimate each polar scattering angle required in the MC calculations, the following accumulation function was used:

$$R(E,\theta) = \frac{\int_0^{\theta} \frac{d\sigma(E)}{d\theta'} d\theta'}{\int_0^{\pi} \frac{d\sigma(E)}{d\theta'} d\theta'} \tag{3a}$$

where

$$\frac{d\sigma}{d\theta} = 2\pi \left(\frac{d\sigma}{d\Omega} \right)_{\theta} \sin\theta \tag{3b}$$

and $d\Omega$ is an element of solid angle. For a given random number r $(0 \le r \le 1)$, the scattering angle θ is chosen so that it satisfies the equation $R(E,\theta) = r$.

In the calculation of the path-length distributions, each electron in the solid is tracked until it is scattered out of the target or until its total path length becomes larger than 6λ, where the IMFP λ for the particular target and energy was estimated from the TPP-2M equation:[7]

$$\lambda = \frac{E}{E_p^2[\beta \ln(\gamma E) - (C/E) + (D/E^2)]} \quad \text{(Å)} \tag{4a}$$

$$\beta = -0.10 + 0.944/(E_p^2 + E_g^2)^{0.5} + 0.069\rho^{0.1} \tag{4b}$$

$$\gamma = 0.191\rho^{-0.5} \tag{4c}$$

$$C = 1.97 - 0.91U \tag{4d}$$

$$D = 53.4 - 20.8U \tag{4e}$$

$$U = N_v \rho / M = E_p^2 / 829.4 \tag{4f}$$

where ρ is the density (g cm^{-3}), N_v is the number of valence electrons per atom, M is the atomic weight, E_g is the band-gap energy (eV) for nonconductors, and E is expressed in eV. The elastically backscattered electrons emitted from the target within the acceptance solid angle of the CMA were counted to obtain the path-length distribution, $d\eta/dS$. These distributions contained at least 10^4 electrons, and the relative precision was thus < 1 %.

RESULTS AND DISCSSION

Energy dependence of measured elastic-peak intensity ratios

The ratios of measured elastic-peak intensities for graphite, Si, Cr, Fe, Cu, Zn, Ga, Mo, Ag, Ta, W, Pt and Au to the corresponding intensities for the Ni reference are shown in Fig. 1(a)-(c) as functions of electron energy. From these Figures, we can see that the energy dependences of the elastic-peak intensity ratios can be classified into four groups according to the relative difference of the atomic numbers to that of Ni. These groups are the low-atomic-number elements (C, Si), the medium-atomic-number elements (Cr, Fe, Zn, Cu, Ga), the upper-medium-atomic-number elements (Ag, Mo), and the high-atomic-number elements (W, Ta, Pt, Au). The similarities in the energy dependences for these groups result from the similar shapes of the differential elastic-scattering cross sections as a function of polar scattering angle for elements of similar atomic numbers.

For Si, in the low-atomic-number group, the intensity ratio monotonically decreased with increasing electron energy from 2 to 0.2. On the other hand, the intensity ratios for Cu were almost constant (about 0.7-1.0) for all measured energies because its atomic number is close to that of Ni; other members of the medium-atomic-number group show similar trends of the intensity ratios. The energy dependence of the intensity ratios for Ag in the upper-medium-atomic-number group, is more complicated. For E > 500 eV, the ratio increased from 0.4 to 2.0. For E < 500 eV, the intensity ratio showed a local maximum at around 200 eV and, for E < 100 eV, increased with decreasing electron energy. The ratios for Au and Pt also showed complicated energy dependences and larger ranges of the ratios (0.2 to over 4.0) than for Ag.

IMFPs determined from elastic-peak intensity ratios

IMFPs for graphite, Si, Cr, Fe, Cu, Zn, Ga, Mo, Ag, Ta, W, Pt, and Au were determined from the measured intensity ratios in Fig. 1 and the dependence of the calculated ratios from Eq. (1) on λ. These IMFPs, designated EPES-IMFP, are shown in Figs. 2-14 as functions of electron energy. Figures 2-14 also show the corresponding IMFPs calculated from energy-loss functions derived from optical data[4,9,10,11] (designated optical IMFPs) and IMFPs from Eq. (4) (designated TPP-2M).

The EPES-IMFPs of Cu, Ag, W and Pt in Figs. 6, 10, 12, and 13 are in excellent agreement with the optical and TPP-2M IMFPs over the 100 eV to 5000 eV energy range. The EPES-IMFPs for Au in Fig. 14 agree well with the optical and TPP-2M IMFPs for the 200 eV to 5000 eV range, but there are disagreements with the optical IMFPs at lower energies. The EPES-IMFPs for Cr, Fe and Ta in Figs. 4, 5, and 11 are in good agreement with the optical IMFPs between 50 eV and 2000 eV, but these IMFPs were smaller than the optical and TPP-2M IMFPs at higher energies.

The EPES-IMFPs for Si in Fig. 3 agreed well with the optical and TPP-2M IMFPs for energies between 100 eV and 1000 eV, but were larger than the latter values at higher energies. These differences could be associated with the fact that our EPES measurements were made with a single-crystal Si specimen. Although the Si surface was amorphized to some extent by sputtering with 250 eV Ar^+, the depth of the sputter-damaged region is probably less than the information depth (ID) for the EPES measurements for $E > 1000$ eV. The ID for 95 %, say, of the detected EPES signal is roughly comparable to the IMFP.[17] For $E > 1000$ eV, the Si IMFP is > 25 Å. Further experiments should be performed with higher ion energies to determine whether this explanation is correct. We also point out that the surface correction factor f_S for Si is expected to be different from that for Ni both in magnitude and in its energy dependence because Si is a typical free-electron-like material and Ni is a typical transition metal. This factor could account for the differences of the EPES-IMFPs from the optical and TPP-2M IMFPs for $E < 100$ eV. Nevertheless, the energy dependence of the Si EPES-IMFPs for energies between 100 eV and 5000 eV resembles those of the optical and TPP-2M IMFPs.

The factors just discussed for Si should also be applicable to the EPES-IMFPs of graphite in Fig. 2. For $E \geq 800$ eV, there are increasing differences of the EPES-IMFPs from the optical IMFPs with increasing energy. The disagreements between the optical and TPP-2M IMFPs are discussed elsewhere.[10] It is thus possible

that the apparent agreement between the EPES and TPP-2M IMFPs in Fig. 2 is fortuitous. For E < 100 eV, there is some scatter in the EPES-IMFP data, particularly at 60 eV, that obscures any trend.

The EPES-IMFPs for Mo in Fig. 9 show a different energy dependence than those of the optical and TPP-2M IMFPs. We have no explanation for this unexpected result.

The EPES-IMFPs for Zn and Ga in Figs. 7 and 8 are in excellent agreement with the corresponding TPP-2M IMFPs. No optical IMFPs are shown in these Figures because optical energy-loss functions are not available.

Analysis of EPES-IMFPs with Fano plots

We have analyzed the EPES-IMFPs shown in Figs. 2-14 using Fano plots. Such plots are useful for checking whether sets of calculated or measured IMFPs are consistent with the Bethe equation describing the total inelastic scattering cross section of electrons in matter.[18] This equation can be written in the form:[3]

$$E / \lambda = E_p^2 \beta \ln(\gamma E) \qquad (5)$$

where E_p is the free-electron bulk plasmon energy and β and γ are parameters. Fano plots are constructed by plotting values of E/λ *versus* $\ln E$. If such a plot is linear, the IMFP data are consistent with the Bethe equation, and values of β and γ can be determined from least-squares fits using Eq. (5).

Our Fano plots are shown in Figs. 15-17 where the symbols indicate values of E/λ (from the EPES-IMFPs) and the lines indicate fits using Eq. (5). We see from the Fano plots for Fe and Cr in Fig. 15 that the E/λ data lie close to the straight lines over the 50 eV to 5000 eV range. For the Fano plot of Si in Fig. 15, the E/λ values could be fitted by a straight line for E > 200 eV. The Fano plot for graphite in Fig. 15 is qualitatively similar to that for Si. We also comment that deviations of the E/λ data for Si and graphite from the straight lines, particularly for energies less than 200 eV, might be due to differences in the surface-electronic excitations for these solids and for Ni and/or to residual crystallinity effects (particularly for graphite), as discussed previously.

The E/λ data in the Fano plots for Cu, Ga, and Mo in Fig. 16 lie close to the

straight lines over the 50 eV to 5000 eV energy range. For Zn, we see unexpected deviations of the E/λ data from the line in the 300 eV to 800 eV region and at high energies. These deviations are discussed further below.

Figure 17 shows Fano plots for Ag, Ta, W, Pt, and Au. Although the E/λ data values lie reasonably close to the lines for each solid over the 50 eV to 5000 eV range, systematic deviations (waviness) are visible, particularly between about 100 eV and 1000 eV. These deviations are also discussed below.

Since the data points in Figs. 15-17 generally lie close to the straight lines for all measured solids, fits were made with Eq. (5) to the data for energies between 50 eV and 5000 eV. Values of the resulting fitting parameters β and γ are listed in Table 1 together with their standard deviations. Table 1 also shows the root-mean-square (RMS) deviations in each fit when the deviations were determined from a minimum energy E_{min} of 50 eV, 100 eV, or 200 eV to a maximum energy of 5000 eV. The average RMS deviations are shown in the final row of Table 1. RMS deviations larger than 20 % are found for graphite, Si, Zn, and Ga when $E_{\min} = 50$ eV. These large deviations are mainly responsible for the average RMS deviation of 18.3 %, again for $E_{\min} = 50$ eV. If E_{min} is increased to 100 eV or 200 eV, the average RMS deviations are reduced to 9.1 % and 7.5 %, respectively. The latter two values are acceptably small for many applications. Equation (5) can then be rearranged to enable the convenient determination of IMFPs from our experiments:

$$\lambda = \frac{E}{E_p^2 \beta \ln(\gamma E)} \qquad \text{(Å)} \qquad (6)$$

with use of the values of E_p, β, and γ in Table 1.

The repeatability of elastic-peak measurements with the CMA was better than 5 %.[13] The standard uncertainty of IMFPs computed from Eq. (6) and the parameters in Table 1 for electron energies between 100 eV and 5000 eV is estimated to be 10 %.

Comparisons of EPES-IMFPs with optical and TPP-2M IMFPs

The RMS differences of IMFPs calculated from Eq. (6) and the parameters in Table 1 with respect to the optical and TPP-2M IMFPs for energies between 100 eV and 5000 eV are shown in Table 2. IMFPs from each data source were calculated at equal

energy intervals on a logarithmic scale corresponding to increments of 10 %. RMS differences were also computed with respect to the optical IMFPs for $E_{\min} = 200$ eV.

Table 2 shows excellent agreement of the IMFPs from the EPES experiments with the optical IMFPs for Si, Cr, Fe, Cu, Ag, Ta, W, Pt and Au and for energies between 100 eV and 5000 eV. For graphite and Mo, however, the RMS differences between the EPES-IMFPs and the optical IMFPs were 27.0 % and 15.9 %, respectively (for the same energy range). Possible reasons for the large RMS difference for graphite have been discussed elsewhere.[10] Nevertheless, the average RMS differences for the group of eleven elemental solids in Table 2 were 11.0 % and 10.2 % for $E_{\min} = 100$ eV and $E_{\min} = 200$ eV, respectively.

Table 2 shows satisfactory agreement between IMFPs from the EPES experiments and the TPP-2M IMFPs for graphite, Cr, Fe, Cu, Zn, Ga, Ag, Pt, and Au. For Mo, Ta, and W, however, the RMS differences between IMFPs from these two sources were 16.9 %, 26.4 %, and 25.7 %, respectively. The average RMS difference of the IMFPs from the EPES experiments with respect to the TPP-2M IMFPs was 10.7 % for electron energies between 100 eV and 5000 eV. We therefore conclude from the average RMS uncertainties in Tables 1 and 2 that the average uncertainties of optical and TPP-2M IMFPs for our 13 element al solids is about 11 % over the same energy range.

Comparison with EPES-IMFPs of Werner *et al.*

Werner *et al.*[19,20] determined IMFPs from EPES experiments for 24 elemental solids (Be, C, Mg, Al, Si, Ti, V, Mn, Fe, Co, Ni, Cu, Zn, Ge, Mo, Pd, Ag, Te, Ta, W, Pt, Au, Pb, and Bi) and energies between 50 eV and 3400 eV. They also fitted the Bethe equation [Eq. (5)] to their IMFPs using Fano plots and reported the resulting values of β and γ for each fit. We have compared IMFPs for eleven of their solids common to our work (C, Si, Fe, Cu, Zn, Mo, Ag, Ta, W, Pt, and Au) using IMFPs computed from Eq. (6) and their values of β and γ with IMFPs similarly computed from Eq. (6) with the values of β and γ in Table 1. These IMFPs were computed at equal intervals of energy on a logarithmic scale from 200 eV (the lower limit in the analysis of Werner *et al.*) to 5000 eV with energy increments of 10 %. The RMS differences between IMFPs from the two calculations for a particular element varied between 3.0 % and 9.0 % for ten of the solids and was 21.6 % for Zn. The average RMS difference was 8.0 % (or 6.6 % if

the results for Zn were excluded). There is thus generally very good agreement between our IMFP results and those of Werner *et al*. Further experiments are needed to determine the origin of the relatively large RMS difference found for Zn. Since this element has a relatively large vapor pressure and will sublime in vacuum, the topography and residual crystallinity of the Zn surfaces in the two experiments might have been different.

Figures 18 and 19 show values of β and of γ obtained from our IMFPs (Table 1) and from the IMFPs of Werner *et al*.[19,20] (denoted β_{EPES} and γ_{EPES}, respectively) versus the corresponding values obtained from fits of Eq. (5) to the optical IMFPs calculated by Tanuma *et al*.[3] for electron energies between 200 eV and 2000 eV (denoted β_{TPP} and γ_{TPP}, respectively). The dashed lines in Figs. 18 and 19 indicate the dependences expected if $\beta_{EPES} = \beta_{TPP}$ and $\gamma_{EPES} = \gamma_{TPP}$. Figure 18 shows that there is generally good agreement between our β values and those of Werner *et al*., although there are outliers from the dashed line for Mo (both sets of data), marginally for Au (Werner *et al*. data), and Ta (our data). Equation (6) indicates that the IMFP is directly proportional to β. For Si, Fe, Cu, Ta, and Au, the differences between our β_{EPES} values and those of Werner *et al*. range from 16.3 % to 29.5 %. Nevertheless, the RMS differences between the IMFPs from Eq. (6) for these solids are much smaller (ranging from 4.8 % to 9.6 %) due to correlation between the values of β_{EPES} and γ_{EPES} in each fit.

Figure 19 shows much larger scatter of the γ_{EPES} values from the dashed line although the differences for the Werner *et al*. values are larger than for ours, especially for Au and Cu, as expected from the larger uncertainties of their values of γ_{EPES} (discussed below). We note that our values of γ_{EPES} in Fig. 19 are generally less than the corresponding values of γ_{TPP}. This result may be due in part to the different lower energy limits used in the fits of Eq. (5) (50 eV in the present analysis and 200 eV in the TPP analysis[3]). The inclusion of IMFPs for $E < 100$ eV can modify the slopes of the Fano plots in Figs. 15-17. We also note that the standard deviations in the γ_{EPES} values for C and Si were relatively large (23.3 % and 27.9 %, respectively).

Werner *et al*.[19,20] published Fano plots for Si, Ge, W, and Pt based on the IMFPs found from their EPES experiments and analysis. These Fano plots display some waviness analogous to that found in some of our Fano plots shown in Figs. 15-17. There is no correlation in the energy positions of the maxima in our Fano plots for Si and W and the corresponding plots of Werner *et al*. although there is reasonably close

agreement in these positions in the Fano plots for Pt. Experimental tests are needed to determine whether the waviness in the Fano plots can be correlated with the sputtering conditions (e.g., the ion dose and energy) used to "amorphize" the samples.

Werner *et al*.[19,20] report the "uncertainties" in their determinations of β from their fits of Eq. (5) to their Fano plots. For the eleven solids common to both investigations, these uncertainties ranged from 8.7 % to 36.4 % (as indicated in Fig. 18); in our fits, the corresponding standard deviations (also shown in Fig. 18) varied from 1.7 % to 8.0 % (and the average standard deviation was 4.3 %). Werner *et al*. stated that the error in their determinations of γ was about 100 % for most of their materials; in our fits, the corresponding standard deviations for γ varied from 5.4 % to 27.9 %, as shown in Fig. 19, and the average value was 7.9 %.

Estimate of uncertainty due to surface-electronic excitations

In the MC calculations of elastic-peak intensity ratios, we ignored the ratio of surface-electronic excitation (SEE) correction factors, f_S^x / f_S^{Ni}, in Eq. (1). However, surface-electronic excitations (due mainly to surface plasmons in free-electron-like solids) are known to be important in both EPES and REELS.[14,21,22] Much work has been done to describe surface excitations using dielectric theory, and a few general equations have been proposed.[23-26] The SEE correction factor f_S for EPES can be described as:

$$f_S = \exp(-P_S^{in}) \exp(-P_S^{out}) \tag{7}$$

where P_s^{in} and P_s^{out} are the surface-excitation probabilities (SEP) for electrons entering and leaving the solid, respectively. Werner *et al*.[26] proposed the following formula for estimating the SEP in any material:

$$P_s = \frac{1}{a\sqrt{E}\cos\theta + 1} \tag{8}$$

where θ here is the angle of electron incidence or emission with respect to the surface normal and a is a material parameter. The latter parameter has been determined from

an analysis of REELS data for Si, Fe, Ni, Cu, Mo, Ta, W, and Au, and can be estimated from an empirical equation for other solids:[26]

$$\frac{a}{a_{NFE}} = 0.039\hbar\Omega_p + 0.4 = 1.12\left(\frac{N_v\rho}{M}\right)^{1/2} + 0.4$$

(9)

where $a_{NFE} = 0.173$ eV$^{-1/2}$. Equation (9) was used to determine values of a for graphite, Cr, Zn, Ga, Ag, and Pt.

Figures 20 and 21 show plots of f_S^x / f_S^{Ni} from Eqs. (7)-(9) as a function of electron energy over the 150 eV to 5000 eV range. These Figures show that the SEE correction term for Eq. (1) is less than 10 % in this energy range for all measured elements except Ga and Si. The average differences of f_S^x / f_S^{Ni} from unity were about 5 % for eleven of our solids (i.e., all except Ga and Si). Since the average RMS difference of the curve fits with the simple Bethe equation to the EPES-IMFPs data is about 10 %, the uncertainty of the SEE correction is unlikely to be significant. Further, neglect of the SEE correction is not expected to lead to significant uncertainties in the determination of IMFPs by EPES. This conclusion is also consistent with the analysis of Powell and Jablonski who found reasonable consistency of optical and EPES-IMFPs for Al, Si, Ni, Cu, Ge, Ag, and Au despite not having made SEE corrections to the EPES-IMFPs.[2] In their analysis, the average mean deviation between optical and EPES-IMFPs from various sources was 17.4 %; no obvious systematic deviation was found as a function of electron energy that might be associated with the SEE correction. Nevertheless, the SEE correction for Si and Ga is larger than 10 % for E < 2000 eV. This correction is therefore important for these elements in the EPES experiments made with our CMA configuration.

For a value of λ_x such that $0.8\lambda_x \le \lambda_x \le 1.2\lambda_x$, Eq. (1) can be simplified to become:[14]

$$\left(\frac{I^x}{I^{Ni}}\right) = \frac{f_S^x}{f_S^{Ni}} \frac{\int_0^\infty \left(d\eta/dS\right)^x / N_0^x \exp\left(-S/\lambda_x\right) dS}{\int_0^\infty \left(d\eta/dS\right)^{Ni} / N_0^{Ni} \exp\left(-S/\lambda_{Ni}\right) dS} \approx \frac{f_S^x}{f_S^{Ni}} \frac{\lambda_x}{k}$$

(10)

where k is a constant. From the results of the fits of Eq. (5) to the EPES-IMFPs in Figs. 15-17, values of EPES-IMFPs *with* the SEE correction, λ_x^f, can be estimated from:

$$\lambda_x^f = \left(\frac{f_S^x}{f_S^{Ni}} \right)^{-1} \lambda_x^{f=1} = \left(\frac{f_S^x}{f_S^{Ni}} \right)^{-1} \frac{E}{E_p^2 \beta \ln(\gamma E)} \tag{11}$$

where $\lambda_x^{f=1}$ is the IMFP determined by EPES *without* the SEE correction. Values of the parameters β and γ in Eq. (11) are listed in Table 1. RMS differences of λ_x^f and $\lambda_x^{f=1}$ with respect to the corresponding optical IMFPs for electron energies between 150 eV and 5000 eV are shown in Fig. 22 as a function of atomic number for those eleven of our elemental solids (graphite, Si, Cr, Fe, Cu, Mo, Ag, Ta, W, Pt, and Au) for which optical IMFPs are available. We see that EPES-IMFPs *with* the Werner *et al*.[26] SEE correction for several elements, especially those with high atomic numbers, gave smaller RMS differences compared to EPES-IMFPs *without* the SEE correction. On the other hand, the EPES-IMFPs *with* the SEE correction for other materials with low atomic numbers, particularly graphite and silicon, gave larger RMS differences than those *without* the SEE correction. The average RMS difference *with* the SEE correction was 10.6 % for these solids while the average RMS difference *without* the SEE correction was 10.3 %.

Figure 23 shows RMS differences of λ_x^f and $\lambda_x^{f=1}$ with respect to the corresponding TPP-2M IMFPs for electron energies between 150 eV and 5000 eV as a function of atomic number for our thirteen solids. As for the similar plot in Fig. 22, no clear trend is apparent. The average RMS difference *with* the SEE correction was 10.0 % while the average RMS difference *without* the SEE correction was 10.7 %. We are therefore unable to assess the effectiveness of the Werner *et al*.[26] SEE correction on IMFPs from EPES experiments. As noted previously, this correction is typically less than 10 %, and it can be neglected for many materials. Nevertheless, Figs. 22 and 23 indicate relatively large RMS differences for graphite (in comparison with optical IMFPs), for Si *without* the SEE correction, for Mo, and for Ta and W (in comparison with TPP-2M IMFPs). Further investigations are needed of the extent to which these

differences might be associated with possible variations of the SEE correction due to specimen roughness induced by sputtering, to limitations of the TPP-2M equation,[10] or other factors.

Influence of choice of differential elastic-scattering cross sections in calculations of elastic-peak intensities

It is necessary to choose an appropriate differential cross section for elastic scattering in the MC calculations of elastic-peak intensities. As mentioned earlier, we chose cross sections calculated from the Thomas-Fermi-Dirac (TFD) potential for free atoms although cross sections obtained from the Dirac-Hartree-Fock (DHF) potential[27,28] are believed to be more reliable.[16] In order to determine the effects of our choice of potential on the ratios of elastic-peak intensities (and thus the EPES-IMFP results), we first show the accumulation functions for Si and Ni calculated from Eq. (3) with differential cross sections from the two potentials for energies of 100 eV and 1000 eV. Figure 24 for Si indicates that the accumulation functions derived from the DHF potential are larger than those from the TFD potential at both energies. While the differences between these functions at 1000 eV are relatively small, those at 100 eV are larger. For Ni, Fig. 25 shows that the differences at both 100 eV and 1000 eV are relatively small. Nevertheless, we need to examine the effects of the choice of potential on the elastic-peak ratios since Ni is used as the reference material in our EPES experiments.

We calculated elastic-peak intensities of Si, Ag, and Au relative to those of Ni using both the TFD and DHF potentials for representative energies of 100 eV, 200 eV, 1000 eV, 2000 eV, and 5000 eV for Si, Ni, Ag, and Au. Figure 26 shows that differences in the elastic-peak ratios for the two potentials are typically about 5 % (and less than 10 %) for $E > 1000$ eV. The differences could be larger (between 14 % and 20 %) for the Si and Ag ratios for energies of 100 eV and 200 eV.

Figure 27 shows Fano plots (symbols) based on our measured EPES intensity ratios and on intensity ratios calculated with both TFD and DHF potentials. A Fano plot based on a fit to Au optical IMFPs[4,11] with Eq. 4(a) is also shown. We see systematic deviations of the points for the EPES data from what can be a near-linear dependence (as represented by fits of Eq. (5) to the EPES data and shown as dashed and dotted lines) for energies between 100 eV and 1000 eV. Although the origin of the "waviness"

of the data points in Fig. 27 and in some of the Fano plots of Figs. 15-17 is not understood, it is clear from Fig. 27 that this is not associated with elastic-scattering cross sections computed from the TFD potential. Since the waviness of the data points in Figs. 15-17 occurs only in some of the Fano plots, it is unlikely to result from an instrumental artifact, particularly since there is no correlation in the energies for the maxima and minima for some materials (graphite, Si, Zn, and Ag in Figs. 15-17); there does appear to be a correlation, however, for these energies for Ta, W, Pt, and Au in Fig. 17). We tentatively conclude that the waviness arises from diffraction-like effects resulting from residual crystallinity in some of the specimens. It is possible that sputtering with 250 eV argon ions for times needed to remove surface contamination may not have been sufficient to fully amorphize some samples to at least the information depth for the EPES experiments.[17]

Figure 27 indicates that E/λ values obtained with the TFD potential are in good agreement with those obtained with the DHF potential for $E \geq 600$ eV (the RMS difference between the data values is 5.0 %). For energies between 200 eV and 500 eV, E/λ values from the TFD potential are more than 10 % larger than those from the DHF potential. Nevertheless, the RMS difference between curve fits to the E/λ values (the dashed and dotted lines) for the two atomic potentials is about 6 % for $E \geq 100$ eV (where the RMS difference was computed from fitted values at energies corresponding to the EPES experiments). For $E \geq 200$ eV, the RMS difference of E/λ values from the fit with based on the DHF potential with respect to the Fano plot for the optical IMFPs was slightly smaller (3.0 %) than the corresponding RMS difference for the fit based on the TFD potential (4.2 %).

Our results in Fig. 26 are similar to those of Jablonski *et al*.[16] The latter authors determined IMFPs from MC simulations with differential cross sections from the two potentials for an AuCu alloy and an Au reference, and found that the differences between the resulting IMFPs varied from 5.0 % at 200 eV to 1.3 % at 2000 eV. In another example, however, Jablonski *et al*. reported IMFP differences of up to 17.1 % from MC simulations with differential cross sections from the two potentials for a "worst-case situation" involving an EPES configuration and an electron energy for which there was a deep minimum in the differential cross section for single large-angle scattering of the primary beam into the analyzer. Differences in IMFPs from MC simulations with differential cross sections from the two potentials are thus likely to be

relatively small for energies above 1000 eV; at lower energies, the IMFP differences may be larger depending on the specimen and reference materials, the experimental configuration, and the electron energy.

SUMMARY

We have determined IMFPs for thirteen elemental solids (graphite, Si, Cr, Fe, Cu, Zn, Ga, Mo, Ag, Ta, W, Pt and Au) by elastic-peak electron spectroscopy for electron energies from 50 eV to 5000 eV. The IMFPs were obtained from measurements of elastic-peak intensities with a novel CMA,[13] use of a Ni reference sample, Monte Carlo simulations, and reference IMFPs computed from the Penn algorithm.[3,14] These IMFPs could be fitted to the Bethe equation for inelastic scattering of electrons in matter for energies from 100 eV to 5000 eV. The average RMS deviation in these fits was 9.1 %.

Our IMFPs for Si, Cr, Fe, Cu, Ag, Ta, W, Pt, and Au are in excellent agreement with those calculated from the Penn algorithm (optical IMFPs) for energies between 100 eV and 5000 eV. The RMS differences for graphite and Mo in these comparisons, however, were rather large (27.0 % and 17.2 %, respectively). Nevertheless, the average RMS difference in these comparisons was 11.0 %. Our IMFPs were also compared with IMFPs from the TPP-2M equation;[7] the average RMS difference was 10.7 % for energies from 100 eV to 5000 eV. Relatively large RMS differences were found for Mo (16.9 %), W (26.4 %), and Ta (26.4 %). In addition, our IMFPs were compared with those of Werner *et al.*[19,20] who performed EPES measurements on a group of 24 elemental solids for energies between 50 eV and 3400 eV. These authors reported values of β and γ in fits to their data with Eq. (5). For the eleven solids common to their work and ours (C, Si, Fe, Cu, Zn, Mo, Ag, Ta, W, Pt, and Au), we computed IMFPs from Eq. (6) with both sets of values of β and γ for energies between 200 eV and 5000 eV. The average RMS differences between the two sets of IMFPs was 8.0 % (or 6.6 % if one large RMS difference of 21.6 % for Zn was excluded).

We investigated the magnitude of the correction for surface-electronic excitations on our IMFPs. This correction was found to be less than 10 % for electron energies above 150 eV and for all of our solids except Si and Ga. The average correction for the other eleven solids was 5 %, again for $E > 150$ eV.

We also examined the effects on our derived IMFPs from use in the Monte Carlo simulations of differential elastic-scattering cross sections computed from the

Thomas-Fermi-Dirac and Dirac-Hartree-Fock atomic potentials. For $E \geq 1000$ eV, the differences of computed elastic-peak intensities from the two potentials for Si, Ag, and Au relative to those of Ni were typically 5 % (and less than 10 %). Larger differences were found for the Si , Ag and Au ratios for $E \leq 500$ eV.

The overall consistency we have found between IMFPs determined here by EPES and IMFPs calculated from optical data indicates that that the uncertainty of these IMFPs is about 11 % for electron energies between 100 eV and 5000 eV. The overall consistency with IMFPs from the similar EPES experiments of Werner *et al*.[19,20] was 8.0 % for energies between 200 eV and 5000 eV.

Acknowledgment

We thank Dr. A. Jablonski for providing differential elastic-scattering cross sections computed from the Dirac-Hartree-Fock potential.

REFEERENCES

1. Penn DR. *Phys. Rev. B* 1987; **35**: 482.
2. Powell CJ, Jablonski A. *J. Phys. Chem. Ref. Data* 1999; **28**: 19.
3. Tanuma S, Powell CJ. Penn DR. *Surf. Interface Anal*. 1988; **11**: 577.
4. Tanuma S, Powell CJ, Penn DR. *Surf. Interface Anal*. 1991; **17**: 911.
5. Tanuma S, Powell CJ, Penn DR. *Surf. Interface Anal*. 1991; **17**: 929.
6. Tanuma S, Powell CJ, Penn DR. *Surf. Interface Anal*. 1993; **20**: 77.
7. Tanuma S, Powell CJ, Penn DR. *Surf. Interface Anal*. 1994; **21**: 165.
8. Tanuma S, Powell CJ, Penn DR. *Surf. Interface Anal*. 1997; **25**: 25.
9. Tanuma S, Powell CJ, Penn DR. *Surf. Interface Anal*. 2003; **35**: 268.
10. Tanuma S, Powell CJ, Penn DR. *Surf. Interface Anal*. 2005; **37**: 1.
11. Tanuma S, Powell CJ, Penn DR. to be published.
12. Gergely G.. *Prog. Surf. Science* 2002; **71**: 31.
13. Goto K, Sakakibara N, Sakai Y. *Microbeam Anal*. 1993; **2**: 123; Takeichi Y, Goto K, *Surf. Interface Anal*. 1997; **25**: 17.
14. Tanuma S, Ichimura S, Goto K. *Surf. Interface Anal*. 2000; **30**: 212.
15. Matsumoto M, Kurita Y. *ACM Trans. on Modeling and Computer Simulation* 1992; **2**: 179.
16. Jablonski A, Salvat F, Powell CJ. *J. Phys. Chem. Ref. Data* 2004; **33**: 409.

17. Jablonski A, Powell CJ. *Surf. Sci*. 2004; **551**: 106.
18. Bethe H. *Ann. der Physik* 1930; **5**: 325.
19. Werner WSM, Tomastik C, Cabela T, Richter G, Störi H. *Surf. Sci*. 2000; **470**: L128.
20. Werner WSM, Tomastik C, Cabela T, Richter G, Störi H. *J. Electron Spectrosc. Relat. Phenom*. 2001; **113**: 127.
21. Tougaard S, Kraaer J. Phys. *Rev. B* 1991; **39**: 1651.
22. Yubero F, Fujita D, Ramskov B, Tougaard S. Phys. *Rev. B* 1996; **53**: 9728.
23. Chen YF. *Surf. Sci*. 1997; **380**:199.
24. Oswald R. Doctoral Dissertation. University of Tubingen, 1997.
25. Kwei CM, Wang CY, Tung CJ. *Surf. Interface Anal*. 1998; **26**: 682.
26. Werner WSM, Smekal W, Tomastik C, Störi H. *Surf. Sci*. 2001; **486**: L461.
27. Salvat F, Jablonski A, and Powell CJ. *Comput. Phys. Commun*. 2005; **165**: 157.
28. Salvat F, Jablonski A, and Powell CJ. NIST Electron Elastic-Scattering Cross-Section Database, Version 3.1, National Institute of Standards and Technology, Gaithersburg, Maryland, 2003.

Table 1. Values of E_p and of the parameters β and γ found in the fits of Eq. (5) to the IMFPs from the EPES measurements for each elemental solid and for energies between 50 eV and 5000 eV, and values of root-mean square (RMS) deviations in these fits for three lower-energy limits, E_{min}; the final row shows the average RMS deviations.[a]

Element	E_p	β	γ	RMS Deviation (%)		
	(eV)	($eV^{-1}Å^{-1}$)	(eV^{-1})	E_{min} = 50 eV	E_{min} = 100 eV	E_{min} = 200 eV
graphite	24.9	0.0154 (0.0010)	0.0643 (0.0150)	42.4	10.4	9.0
Si	16.6	0.0323 (0.0026)	0.0655 (0.0183)	56.4	14.3	7.0
Cr	26.1	0.0278 (0.0005)	0.0318 (0.0017)	7.4	5.9	3.6
Fe	30.6	0.0204 (0.0005)	0.0314 (0.0022)	8.5	4.7	3.5
Cu	35.9	0.0136 (0.0005)	0.0392 (0.0056)	5.9	6.1	5.7
Zn	33.0	0.0153 (0.0011)	0.0387 (0.0088)	28.1	12.9	12.3
Ga	14.5	0.0625 (0.0046)	0.0402 (0.0097)	26.0	6.5	7.0
Mo	23.1	0.0410 (0.0008)	0.0259 (0.0014)	8.4	6.2	3.5
Ag	29.8	0.0230 (0.0007)	0.0316 (0.0030)	10.7	11.1	11.7
Ta	19.5	0.0569 (0.0017)	0.0297 (0.0026)	14.6	11.0	6.6
W	22.9	0.0427 (0.0019)	0.0382 (0.0056)	12.4	11.7	10.3
Pt	30.2	0.0255 (0.0010)	0.0341 (0.0044)	9.9	10.5	10.4
Au	29.9	0.0241 (0.0005)	0.0380 (0.0028)	7.0	6.6	6.7
			average RMS deviation:	18.3	9.1	7.5

[a]The numerical values in the parentheses indicate the standard deviations for β *and* γ in the fits to the Fano plots of the IMFP-EPES data in Figs. 15-17.

Table 2. Root-mean-square differences of EPES-IMFPs from Eq. (6) and the parameters in Table 1 with respect to the optical and TPP-2M IMFPs for the indicated elemental solids.[a]

Element	RMS Difference (%)		
	Optical IMFP		TPP-2M IMFP
	$E_{\min} = 100$ eV	$E_{\min} = 200$ eV	$E_{\min} = 100$ eV
graphite	27.0	27.4	8.9
Si	8.9	8.4	11.2
Cr	9.1	9.9	12.7
Fe	7.0	7.6	7.7
Cu	10.7	9.1	1.9
Zn	–	–	5.7
Ga	–	–	12.1
Mo	15.9	17.2	16.9
Ag	3.7	1.7	4.4
Ta	8.7	9.0	26.4
W	11.3	9.8	25.7
Pt	9.1	8.0	2.4
Au	10.0	4.2	3.6
average RMS difference:	11.0	10.2	10.7

[a]Optical IMFPs are not available for Zn and Ga.

Figure Captions

Figure 1. Ratios of measured elastic-peak intensities for the indicated elemental solids to those of Ni as a function of electron energy. (a) graphite, Si, Cr and Fe; (b) Cu, Zn, Ga and Mo; (c) Ag, Ta, W, Pt and Au.

Figure 2. IMFP values (solid circles) for graphite determined from the elastic-peak intensity ratios in Fig. 1 as a function of electron energy. The solid line shows IMFP values calculated from the Penn algorithm using the energy-loss function of graphite. The dotted line shows IMFPs calculated from the IMFP predictive formula TPP-2M (Eq. (4)).

Figure 3. IMFP results for silicon as a function of electron energy (see caption to Fig. 2).

Figure 4. IMFP results for chromium as a function of electron energy (see caption to Fig. 2).

Figure 5. IMFP results for iron as a function of electron energy (see caption to Fig. 2).

Figure 6. IMFP results for copper as a function of electron energy (see caption to Fig. 2).

Figure 7. IMFP values (solid circles) for zinc determined from elastic-peak intensity ratios in Fig. 1 as a function of electron energy. The dotted line shows IMFPs calculated from the IMFP predictive formula TPP-2M (Eq. (4)).

Figure 8. IMFP results for gallium as a function of electron energy (see caption to Fig. 7).

Figure 9. IMFP results for molybdenum as a function of electron energy (see caption to Fig. 2).

Figure 10. IMFP results for silver as a function of electron energy (see caption to Fig. 2).

Figure 11. IMFP results for tantalum as a function of electron energy (see caption to Fig. 2).

Figure 12. IMFP results for tungsten as a function of electron energy (see caption to Fig. 2).

Figure 13. IMFP results for platinum as a function of electron energy (see caption to Fig. 2).

Figure 14. IMFP results for gold as a function of electron energy (see caption to Fig. 2).

Figure 15. Fano plots based on EPES-IMFPs for graphite, silicon, chromium and iron. Values of E/λ (solid symbols) are plotted as a function of energy on a logarithmic scale. The solid lines are fits to the E/λ data with Eq. (5); values of the parameters in the fits are given in Table 1.

Figure 16. Fano plots for copper, zinc, gallium and molybdenum (see caption to Fig.15).

Figure 17. Fano plots for silver, tantalum, tungsten, platinum and gold (see caption to Fig.15).

Figure 18. Plot of β_{EPES} values determined from fits of Eq. (5) to IMFPs determined from EPES experiments versus β_{TPP} values from similar fits to IMFPs calculated from optical data (Ref. 3). The solid circles show the results of the present work (left-hand scale) and the open circles show the results of Werner *et al.*[19,20] (right-hand scale). The dashed lines shows the dependence $\beta_{EPES} = \beta_{TPP}$. The error bars indicate the one-standard-deviation limits in the determinations of β_{EPES}; for some points, these error bars are less than the size of the symbols.

Figure 19. Plot of γ_{EPES} values determined from fits of Eq. (5) to IMFPs determined from EPES experiments versus γ_{EPES} values from similar fits to IMFPs calculated from optical data (Ref. 3). The solid circles show the results of the present work (left-hand scale) and the open circles show the results of Werner *et al*.[19,20] (right-hand scale). The dashed lines shows the dependence $\gamma_{EPES} = \gamma_{TPP}$. The error bars indicate the one-standard-deviation limits in the determinations of γ_{EPES}; for some points, these error bars are less than the size of the symbols.

Figure 20. Ratios of the surface-electronic excitation correction for Si, Fe, Cu, Mo, Ta, W, and Au to that for Ni, f_S^x / f_S^{Ni}, as a function of electron energy.

Figure 21. Ratios of the surface-electronic excitation correction for graphite, Cr, Zn, Ga, Ag, and Pt to that for Ni, f_S^x / f_S^{Ni}, as a function of electron energy.

Figure 22. RMS differences of EPES-IMFPs obtained with (open circles) and without (solid circles) the surface-electronic excitation correction for graphite, Si, Cr, Fe, Cu, Mo, Ag, Ta, W, Pt, and Au with respect to the corresponding optical IMFPs as a function of atomic number. Values of the EPES-IMFPs *with* the SEE correction were obtained from Eq. (11) while values of EPES-IMFPs *without* the SEE correction correspond to 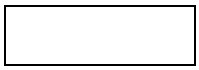 .

Figure 23. RMS differences of EPES-IMFPs obtained *with* (open circles) and *without* (solid circles) the surface-electronic excitation correction for graphite, Si, Cr, Fe, Cu, Zn, Cu, Mo, Ag, Ta, W, Pt, and Au with respect to the corresponding TPP-2M IMFPs as a function of atomic number (see caption to Fig. 22).

Figure 24. Accumulation functions for silicon calculated from Eq. (3) for the Thomas-Fermi-Dirac potential (dotted lines) and the Dirac-Hartree-Fock potential (solid lines) for electron energies of 100 eV and 1000 eV.

Figure 25. Accumulation functions for nickel calculated from Eq. (3) for the Thomas-Fermi-Dirac potential (dotted lines) and the Dirac-Hartree-Fock potential (solid lines) at 100 eV and 1000 eV.

Figure 26. Elastic-peak intensity ratios for silicon, silver, and gold to a nickel reference calculated from Eq. (1) and ☐ using the Thomas-Fermi-Dirac potential (open symbols) and the Dirac-Hartree-Fock potential (solid symbols).

Figure 27. Fano plots based on EPES-IMFPs for gold determined using differential elastic-scattering cross sections from the TFD and DHF potentials. Values of E/λ (symbols) are plotted as a function of energy on a logarithmic scale. The dotted and dashed lines are fits to these E/λ data with Eq. (5). The solid line shows a fit to E/λ values calculated from Au optical IMFPs with Eq. (4a) in which β, γ, C, and D were allowed to vary (Refs. 4 and 11).

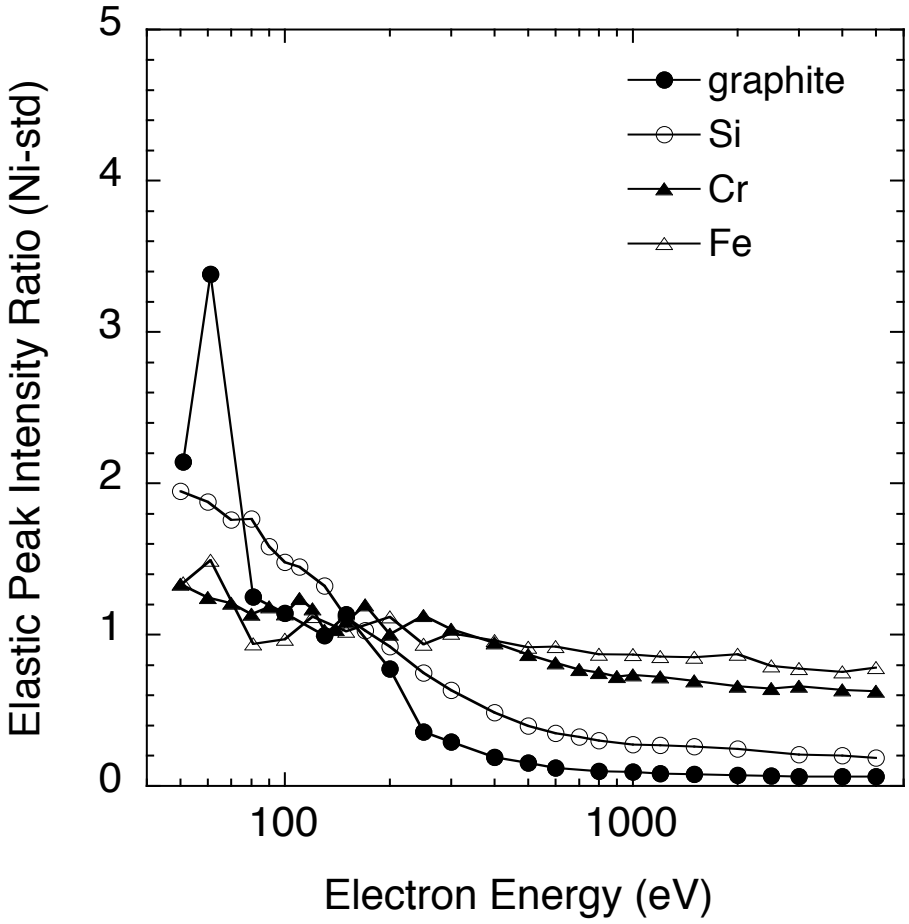
graphite
Si
Cr
Fe
Elastic Peak Intensity Ratio (Ni-std)
Electron Energy (eV)
0
1
2
3
4
5
100
1000

Fig.1-(a)

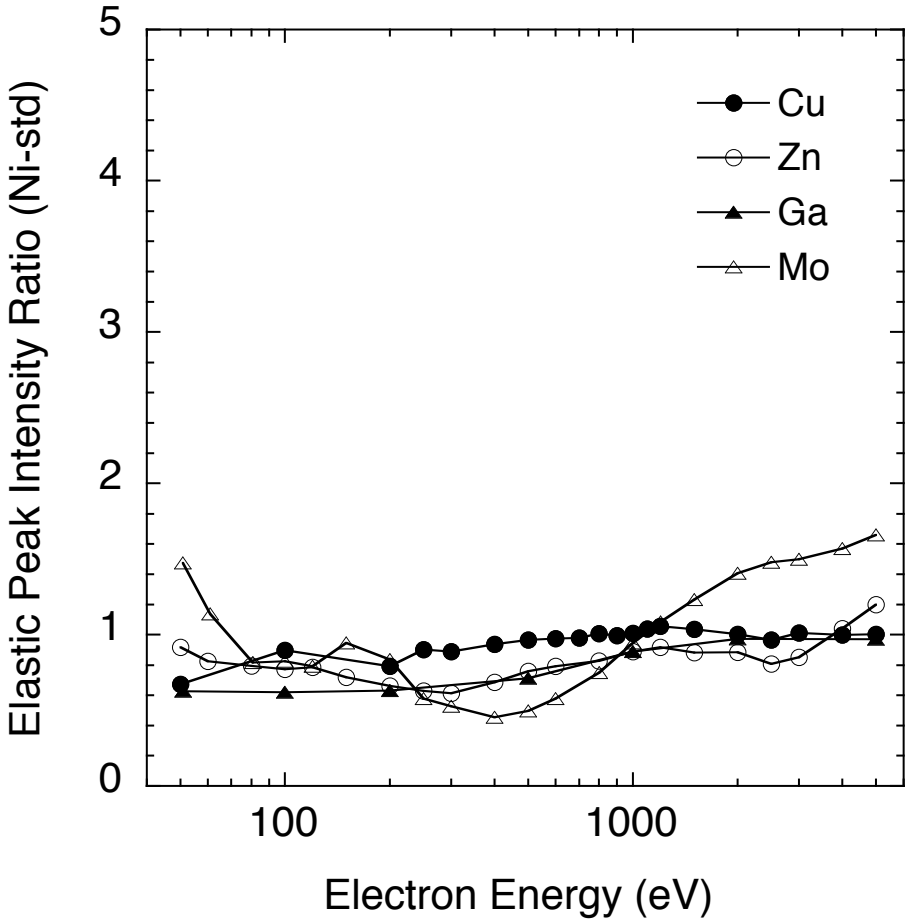
Elastic Peak Intensity Ratio (Ni-std)
Electron Energy (eV)
Cu
Zn
Ga
Mo
0
1
2
3
4
5
100
1000

Fig.1-(b)

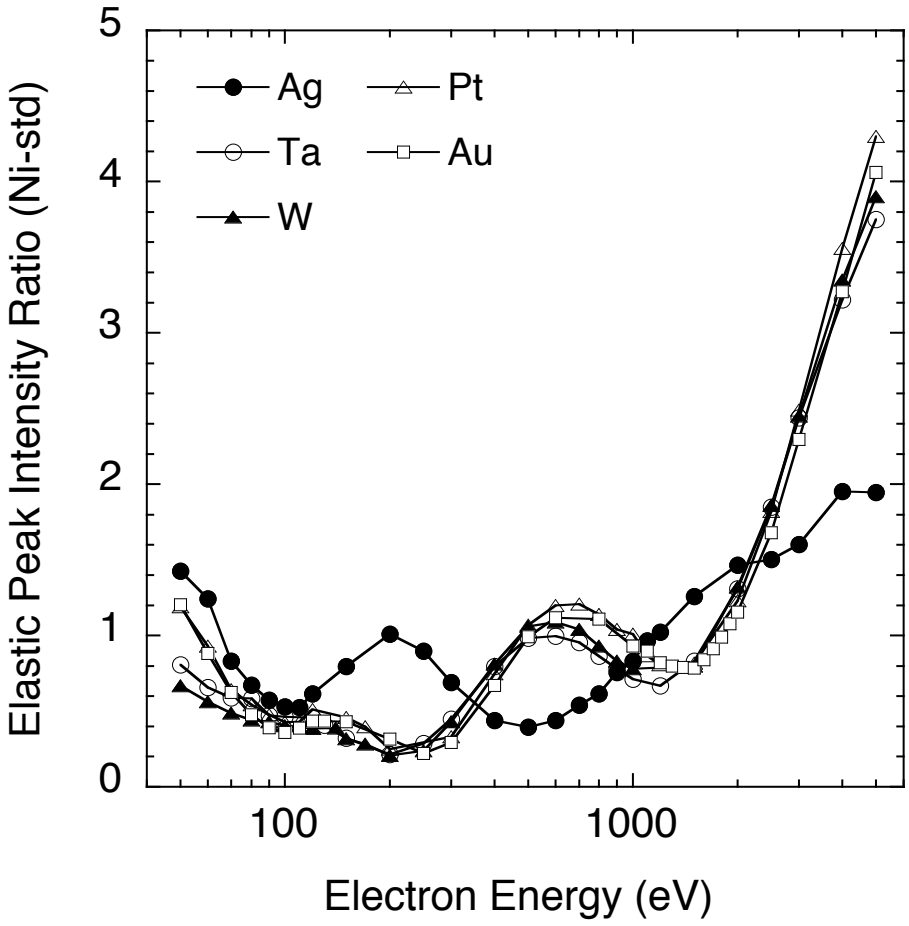
Ag
Pt
Ta
Au
W
Elastic Peak Intensity Ratio (Ni-std)
Electron Energy (eV)
0
1
2
3
4
5
100
1000

Fig.1-(c)

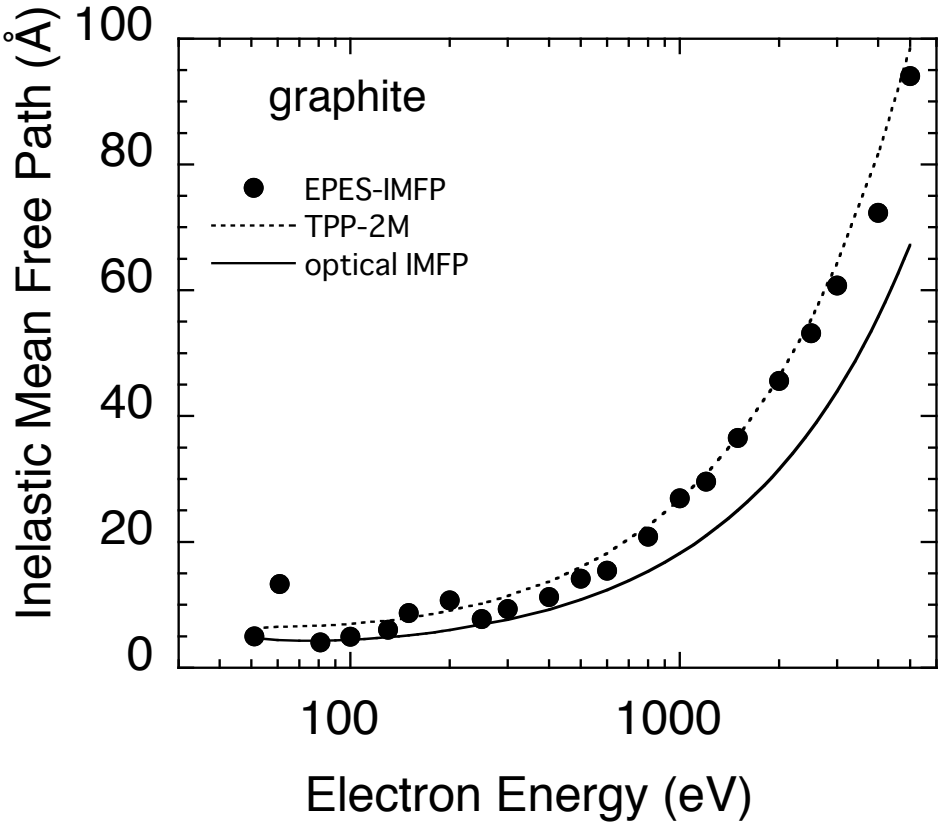
graphite
EPES-IMFP
TPP-2M
optical IMFP
Inelastic Mean Free Path (Å)
0
20
40
60
80
100
100
1000
Electron Energy (eV)

Fig.2

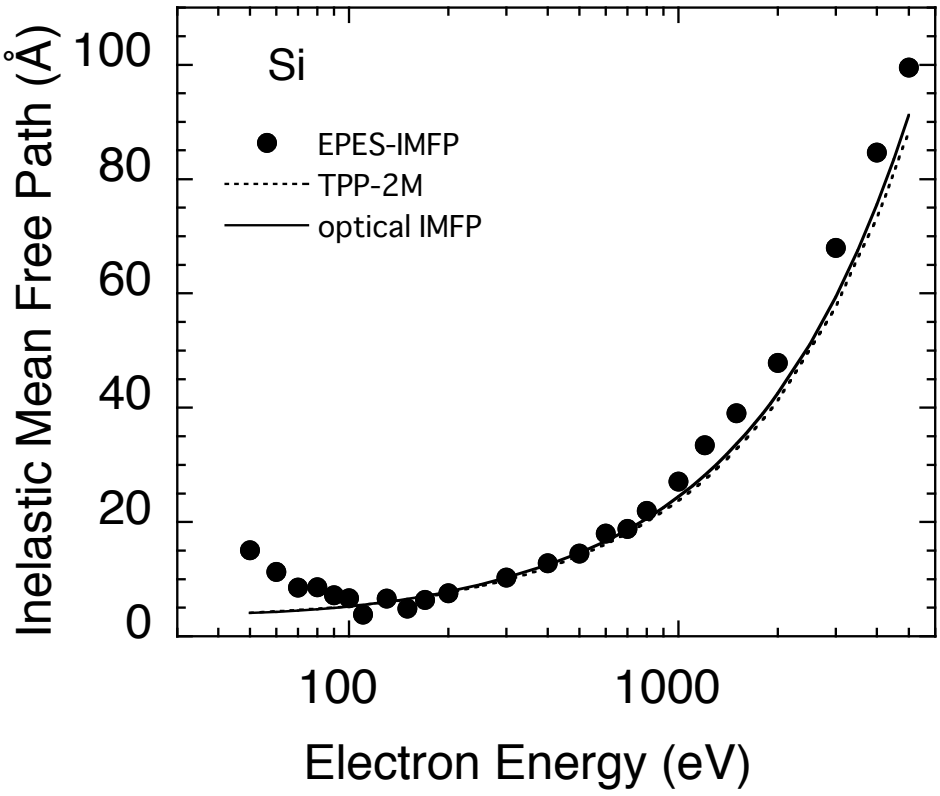
Si
EPES-IMFP
TPP-2M
optical IMFP
Inelastic Mean Free Path (Å)
0
20
40
60
80
100
100
1000
Electron Energy (eV)

Fig.3

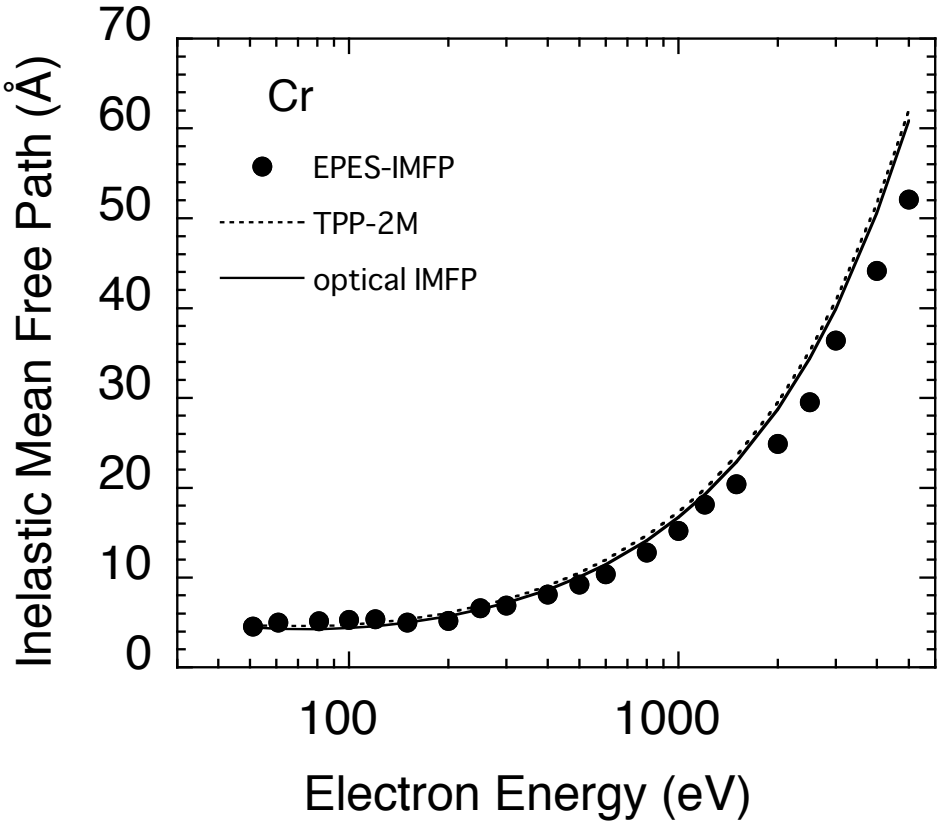
Cr
EPES-IMFP
TPP-2M
optical IMFP
Inelastic Mean Free Path (Å)
Electron Energy (eV)
0
10
20
30
40
50
60
70
100
1000

Fig.4

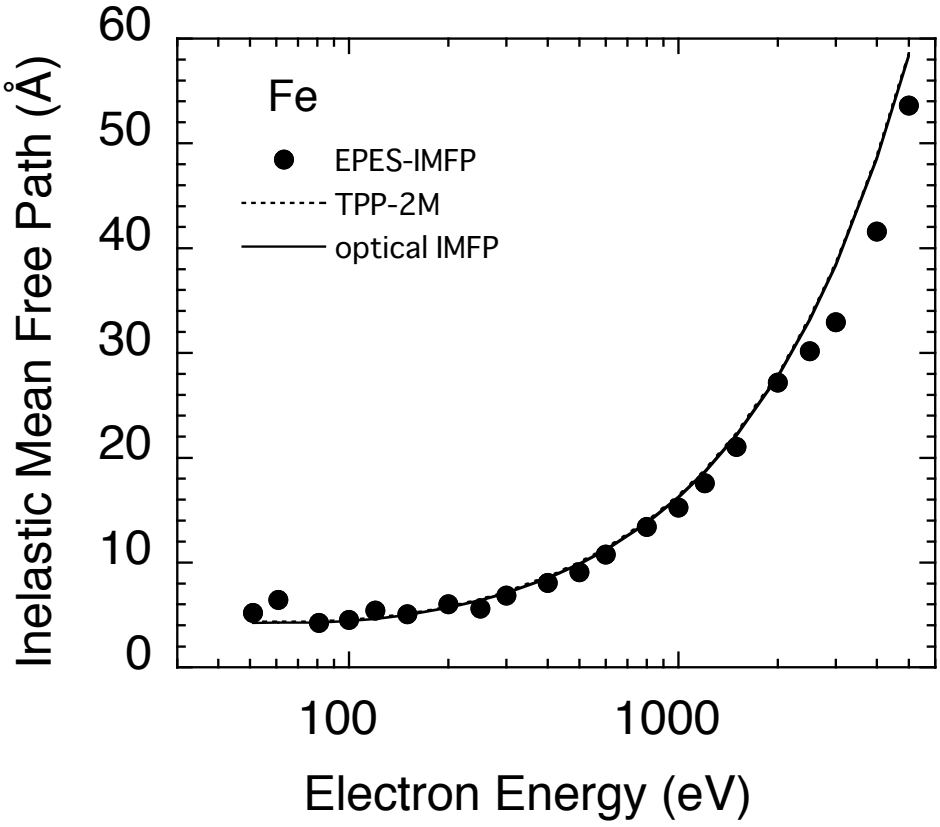
Fe
EPES-IMFP
TPP-2M
optical IMFP
Inelastic Mean Free Path (Å)
Electron Energy (eV)
0
10
20
30
40
50
60
100
1000

Fig.5

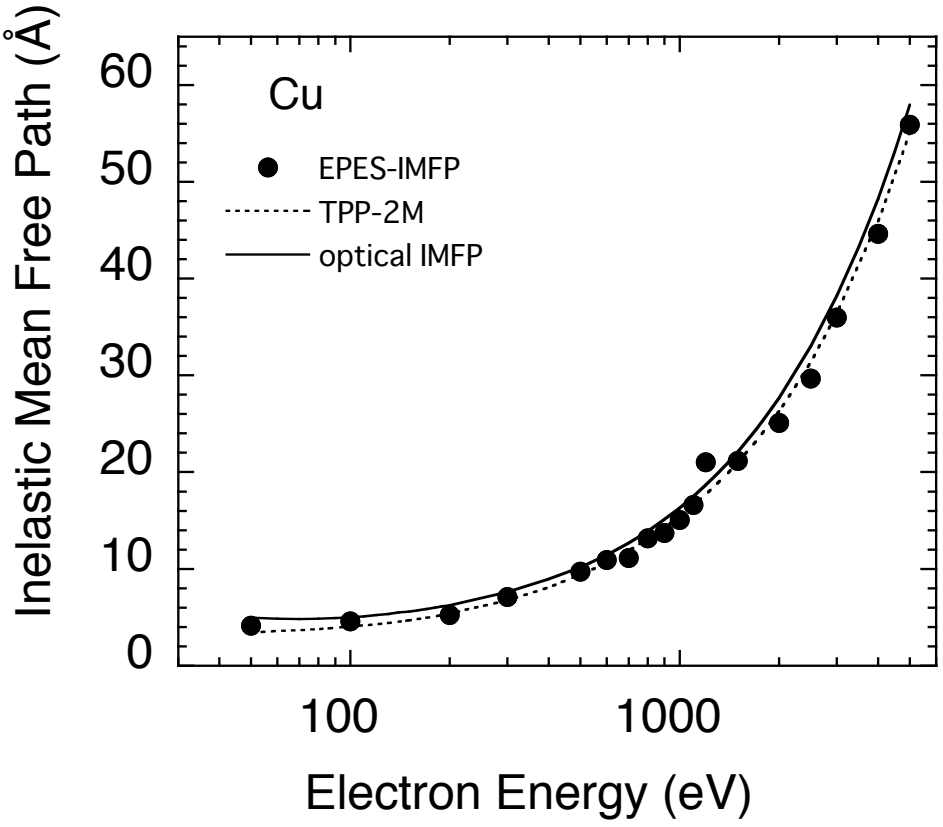
Inelastic Mean Free Path (Å)
60
50
40
30
20
10
0
Cu
EPES-IMFP
TPP-2M
optical IMFP
100
1000
Electron Energy (eV)

Fig. 6

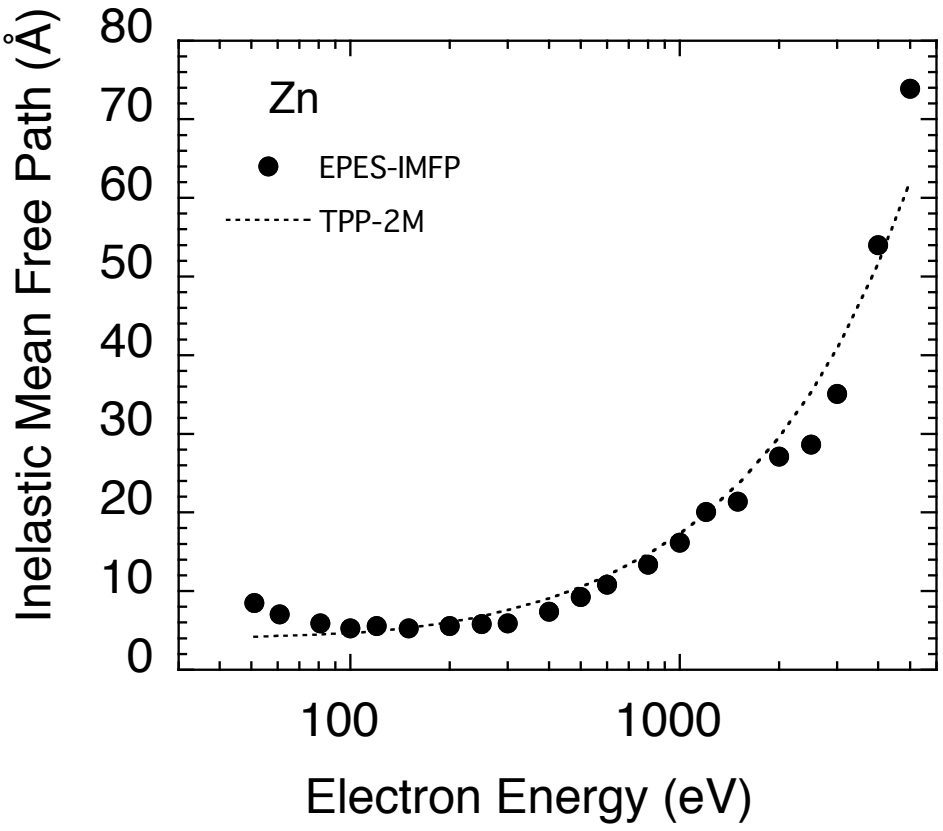
Zn
EPES-IMFP
TPP-2M
Inelastic Mean Free Path (Å)
Electron Energy (eV)
0
10
20
30
40
50
60
70
80
100
1000

Fig. 7

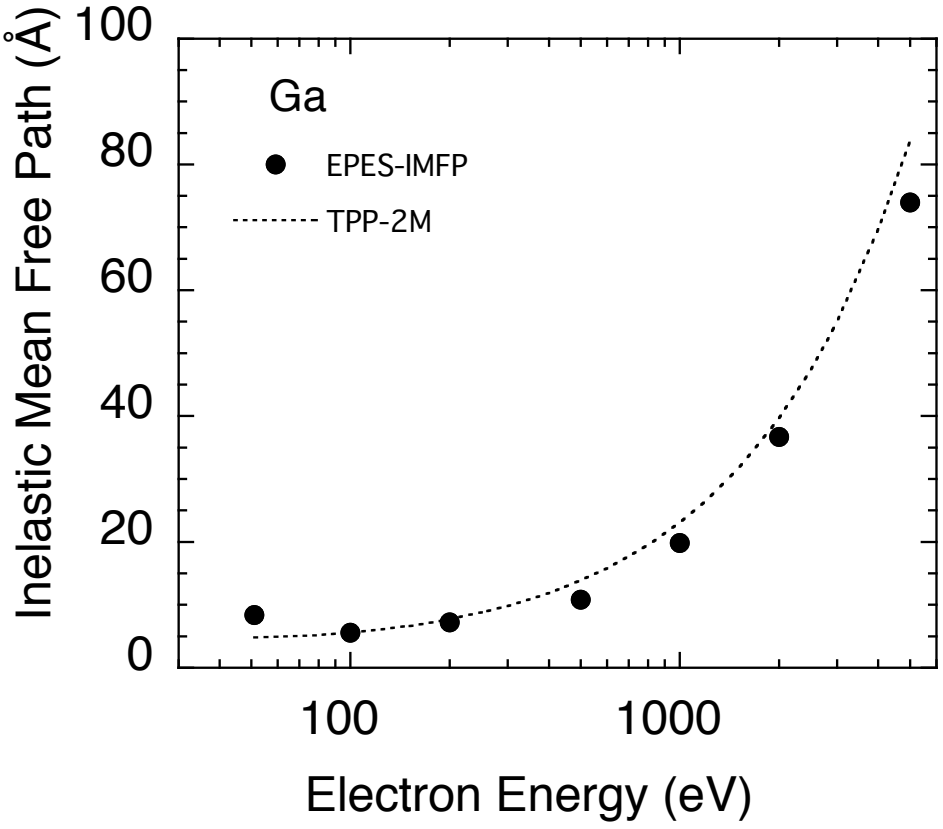
Ga
EPES-IMFP
TPP-2M
Inelastic Mean Free Path (Å)
100
80
60
40
20
0
100
1000
Electron Energy (eV)

Fig. 8

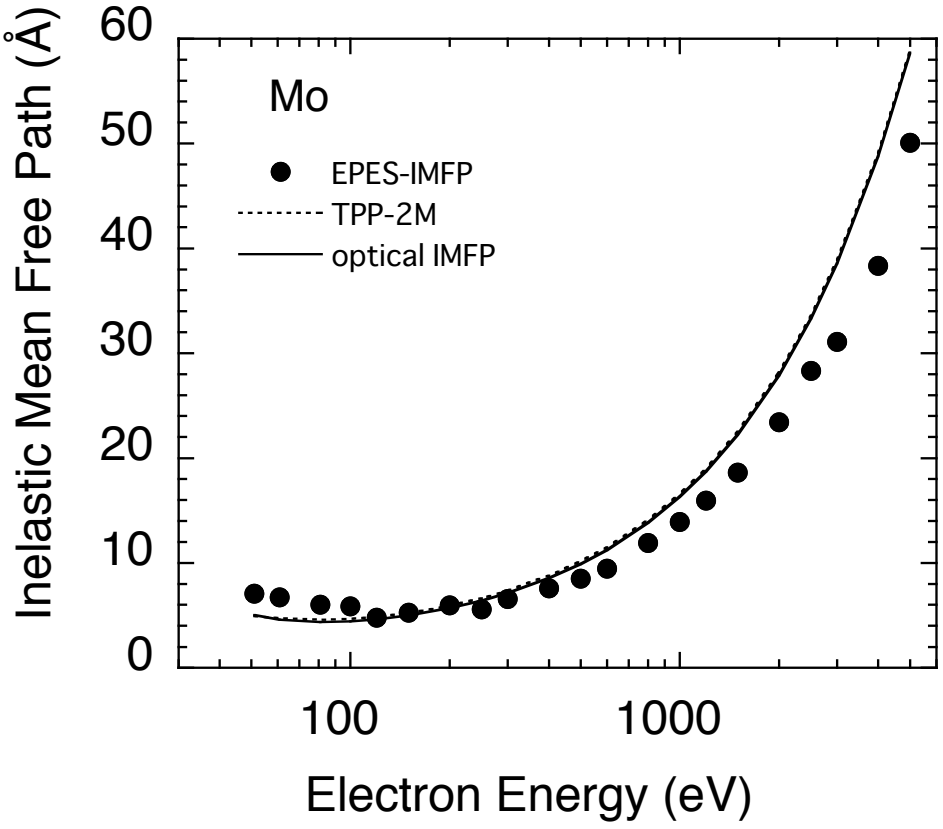
Mo
EPES-IMFP
TPP-2M
optical IMFP
Inelastic Mean Free Path (Å)
Electron Energy (eV)
0
10
20
30
40
50
60
100
1000

Fig. 9

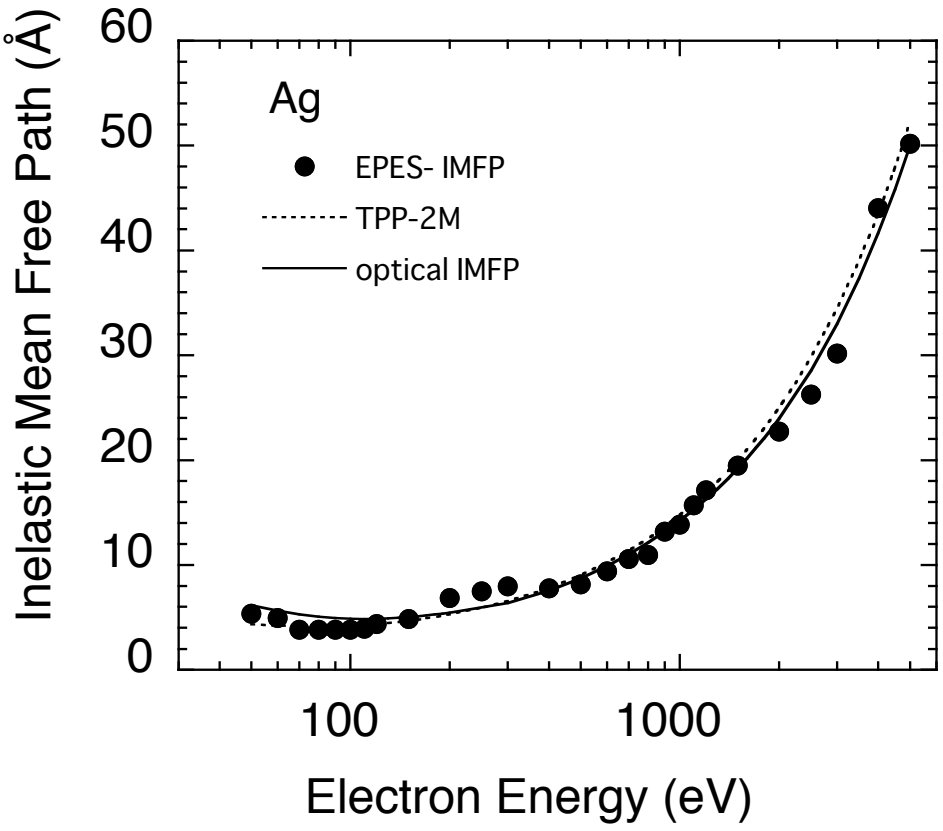
Ag
EPES- IMFP
TPP-2M
optical IMFP
Inelastic Mean Free Path (Å)
Electron Energy (eV)
0
10
20
30
40
50
60
100
1000

Fig. 10

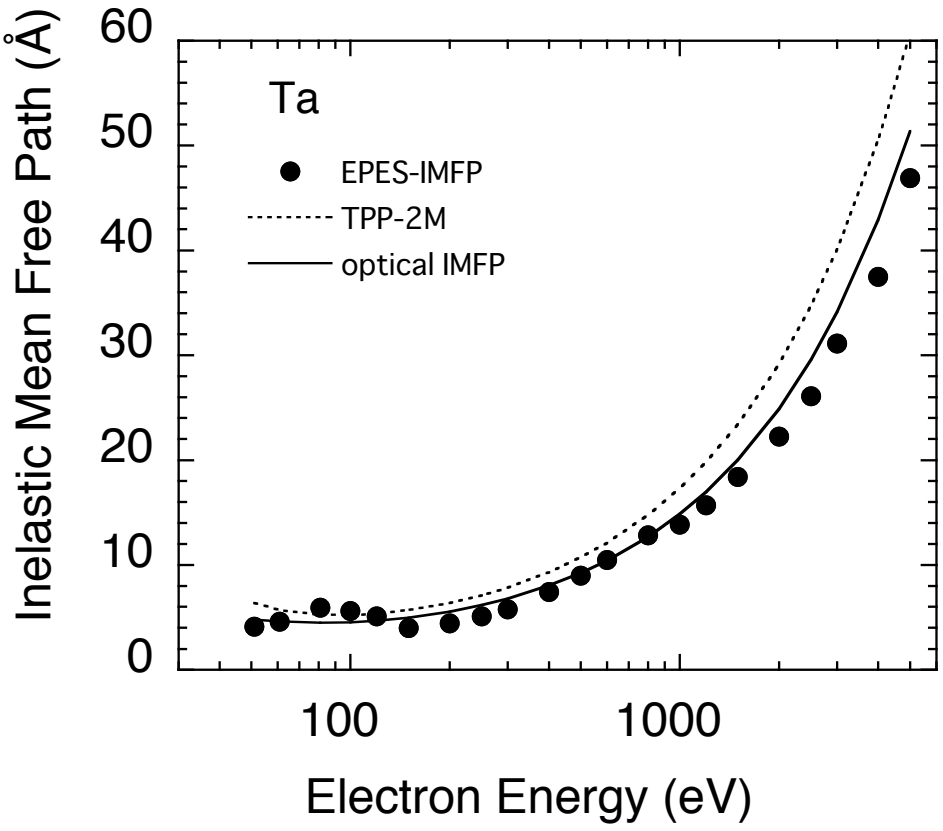
Ta
EPES-IMFP
TPP-2M
optical IMFP
Inelastic Mean Free Path (Å)
Electron Energy (eV)
0
10
20
30
40
50
60
100
1000

Fig. 11

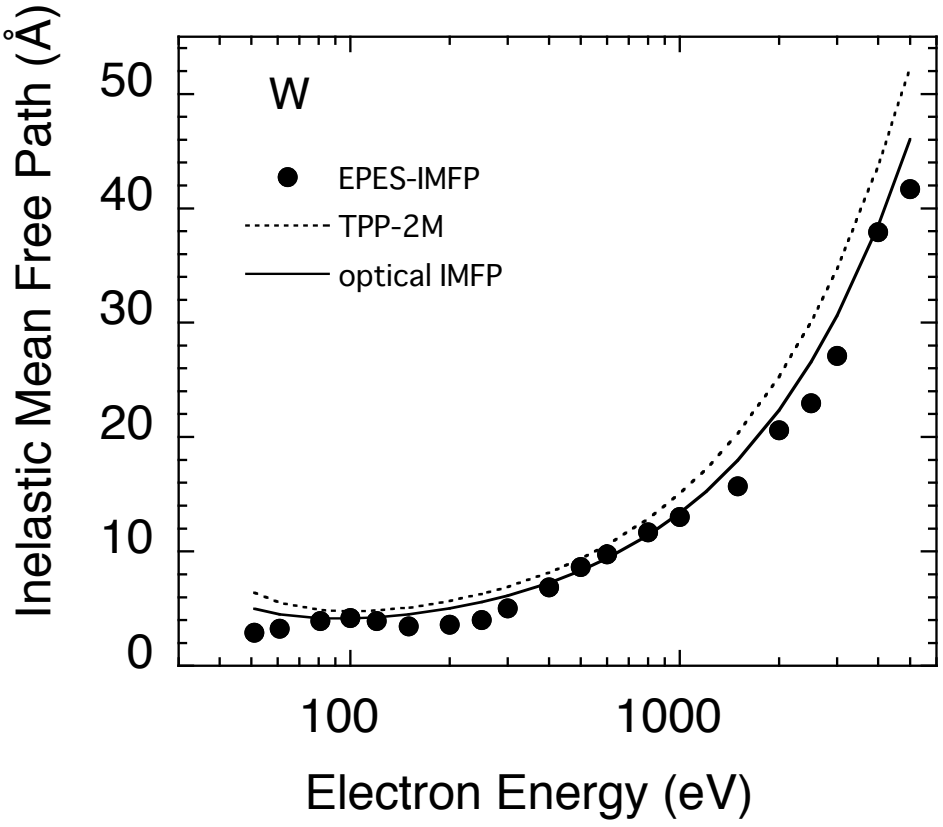
W
EPES-IMFP
TPP-2M
optical IMFP
Inelastic Mean Free Path (Å)
Electron Energy (eV)
0
10
20
30
40
50
100
1000

Fig. 12

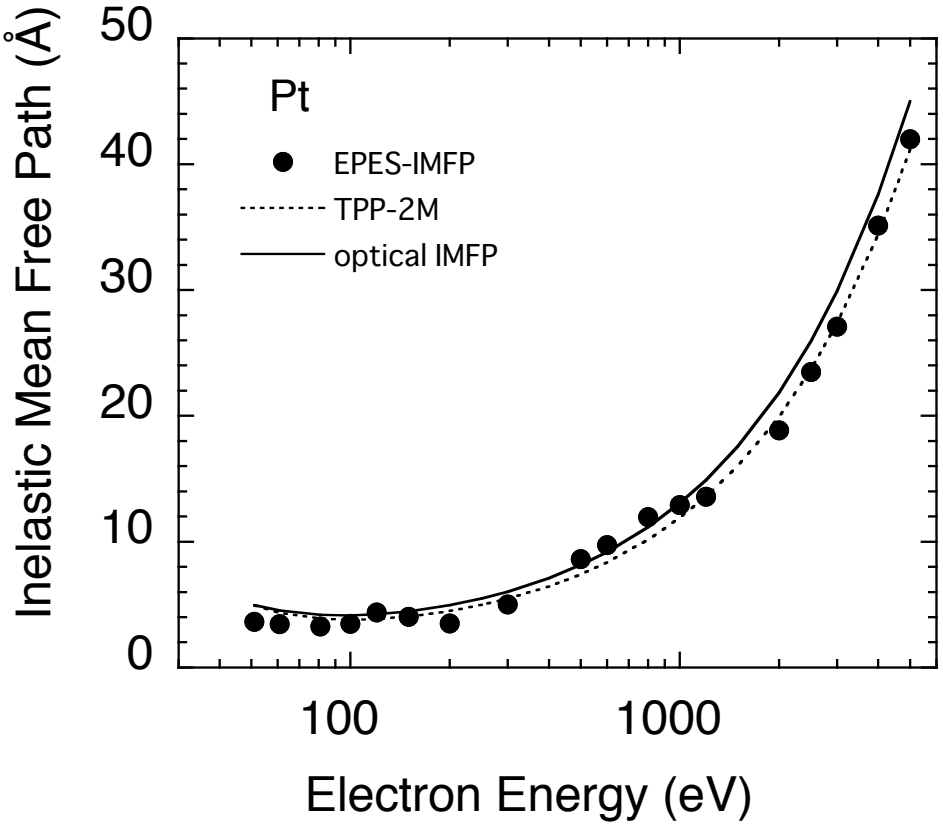
Pt
EPES-IMFP
TPP-2M
optical IMFP
Inelastic Mean Free Path (Å)
Electron Energy (eV)
0
10
20
30
40
50
100
1000

Fig. 13

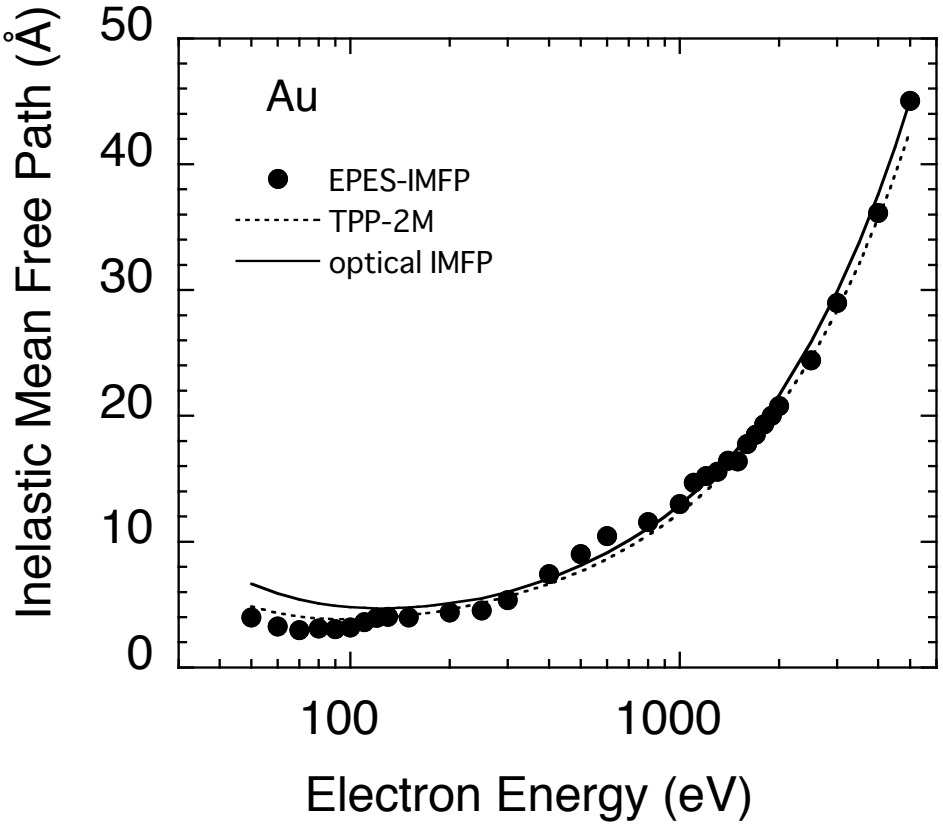
Au
EPES-IMFP
TPP-2M
optical IMFP
Inelastic Mean Free Path (Å)
Electron Energy (eV)
0
10
20
30
40
50
100
1000

Fig. 14

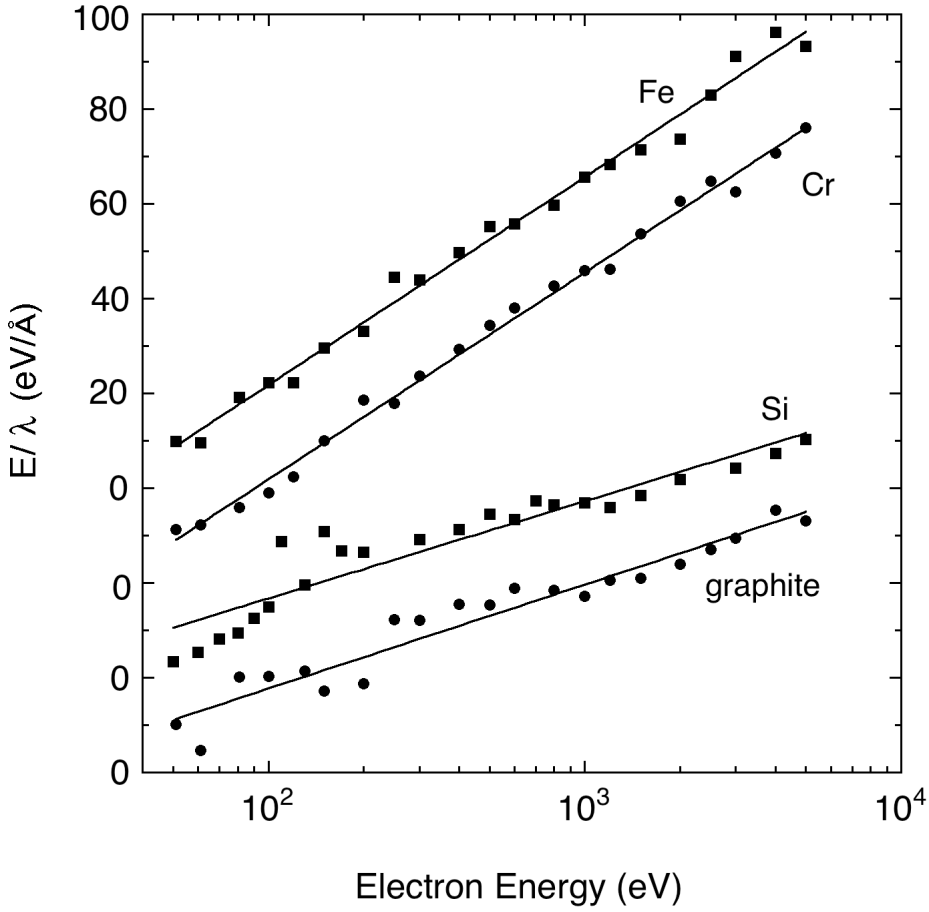
100
80
60
40
20
0
0
0
0
E/λ (eV/Å)
Fe
Cr
Si
graphite
10^2
10^3
10^4
Electron Energy (eV)

Fig15

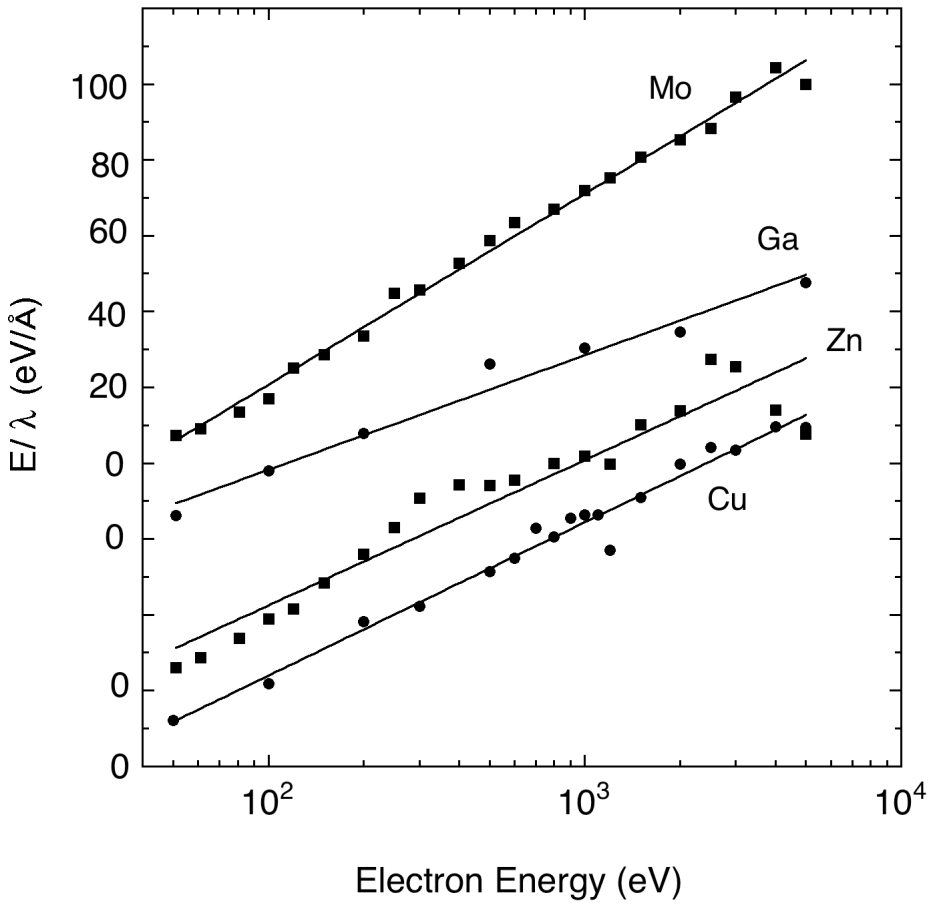
Mo
Ga
Zn
Cu
E/λ (eV/Å)
Electron Energy (eV)
100
80
60
40
20
0
0
0
0
10^2
10^3
10^4

Fig16.

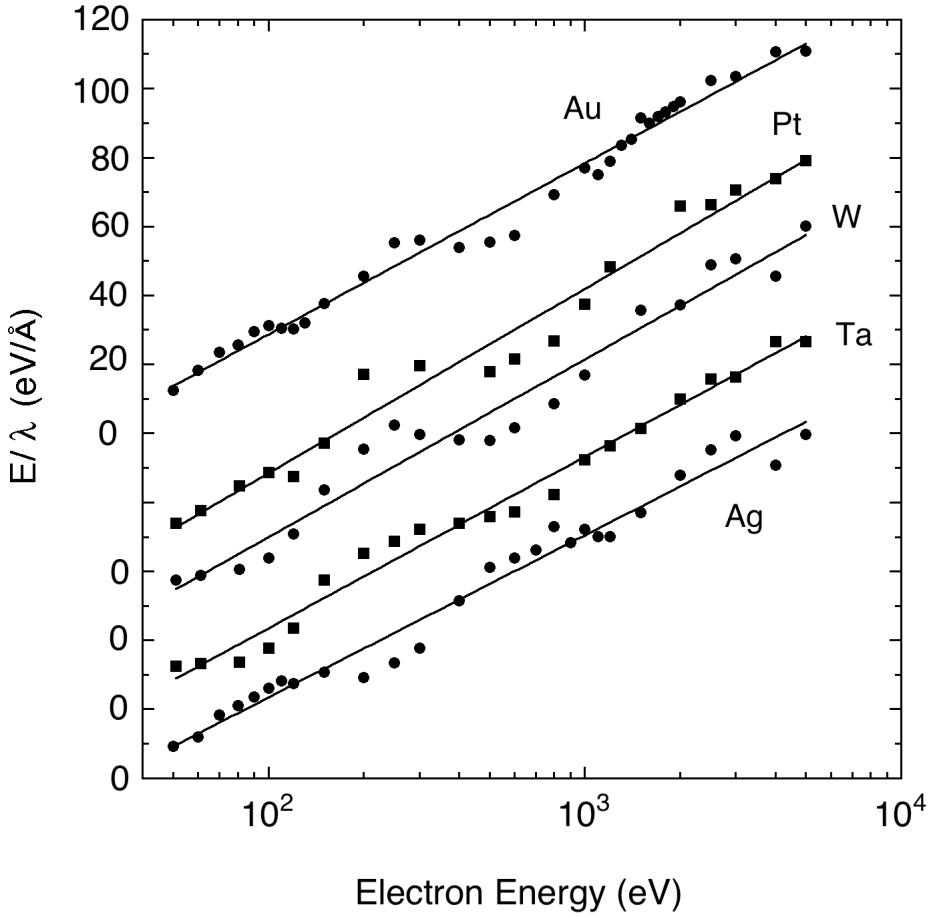
120
100
80
60
40
20
0
0
0
0
0
E/λ (eV/Å)
Au
Pt
W
Ta
Ag
10^2
10^3
10^4
Electron Energy (eV)

Fig. 17

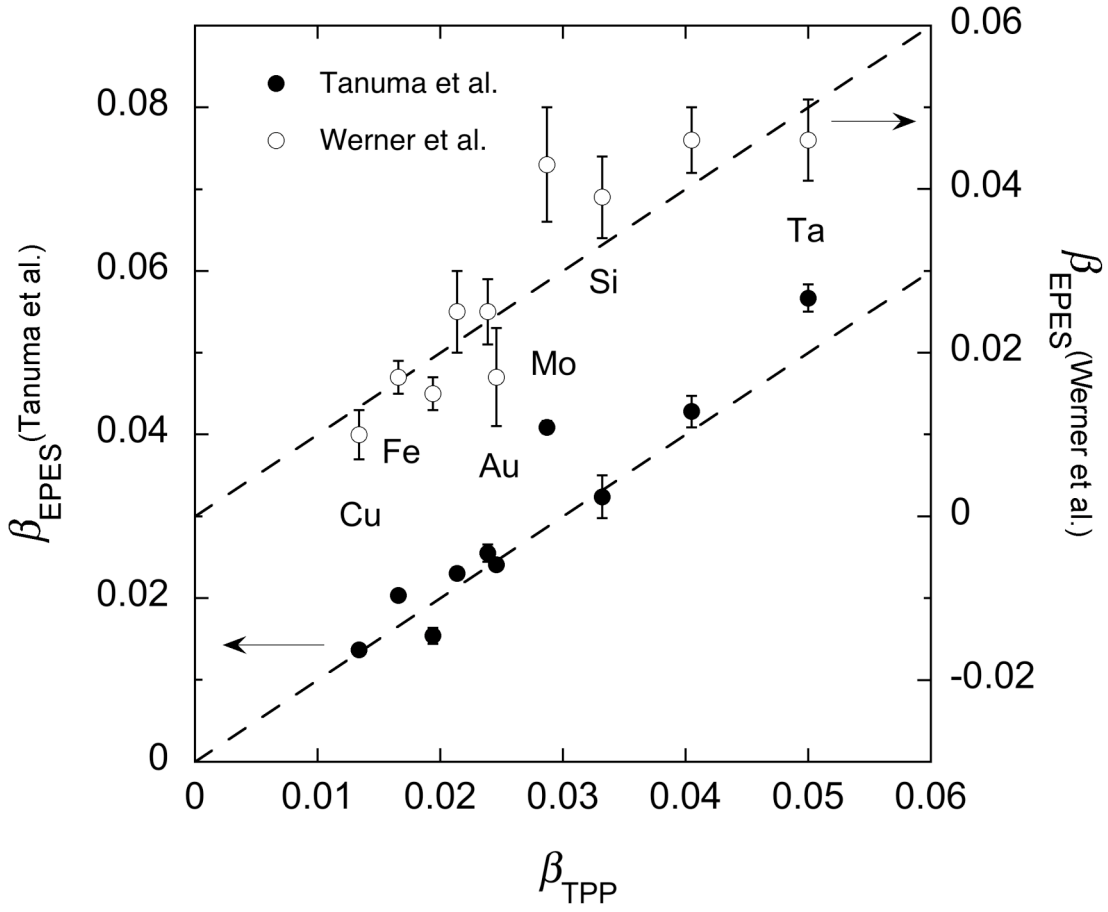
Tanuma et al.
Werner et al.
Cu
Fe
Au
Mo
Si
Ta
0.08
0.06
0.04
0.02
0
0.06
0.04
0.02
0
-0.02
0
0.01
0.02
0.03
0.04
0.05
0.06
β_{EPES}(Tanuma et al.)
β_{EPES}(Werner et al.)
β_{TPP}

Fig. 18

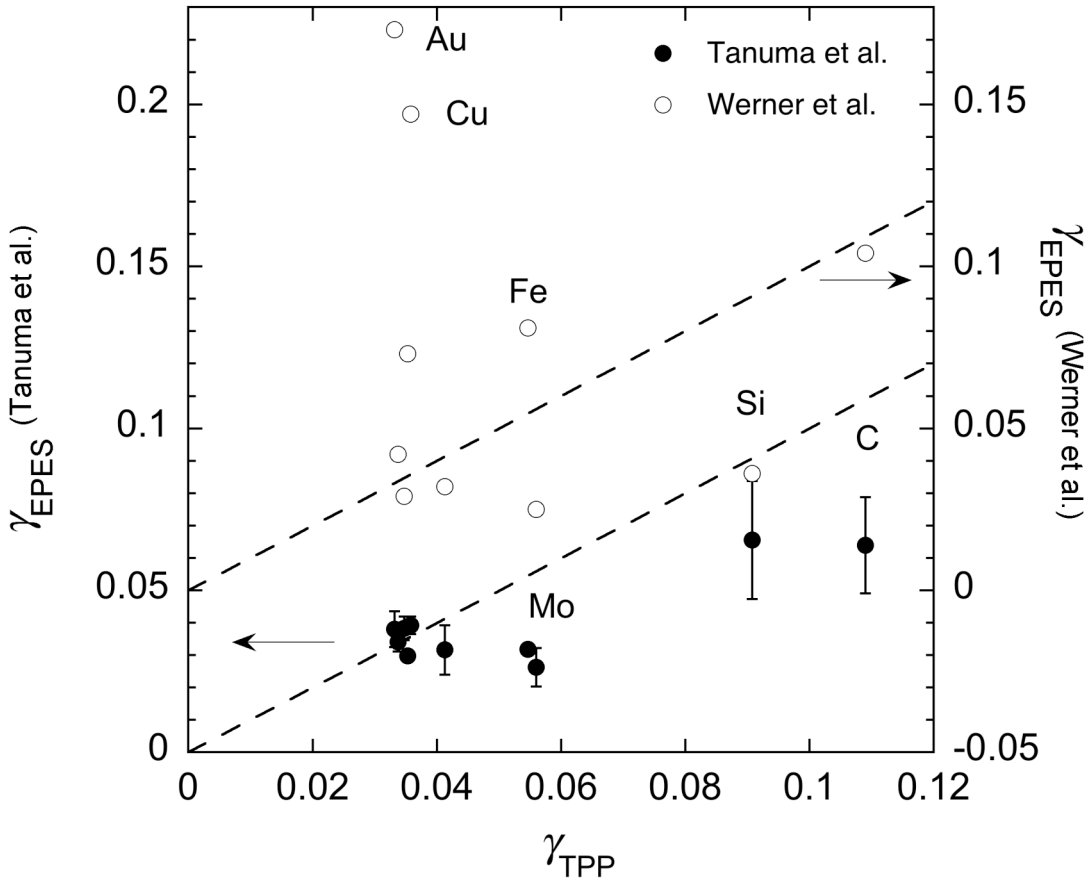
Au
Cu
Fe
Si
C
Mo
Tanuma et al.
Werner et al.
0.2
0.15
0.1
0.05
0
0.15
0.1
0.05
0
-0.05
0
0.02
0.04
0.06
0.08
0.1
0.12
γ_{EPES} (Tanuma et al.)
γ_{EPES} (Werner et al.)
γ_{TPP}

Fig.19

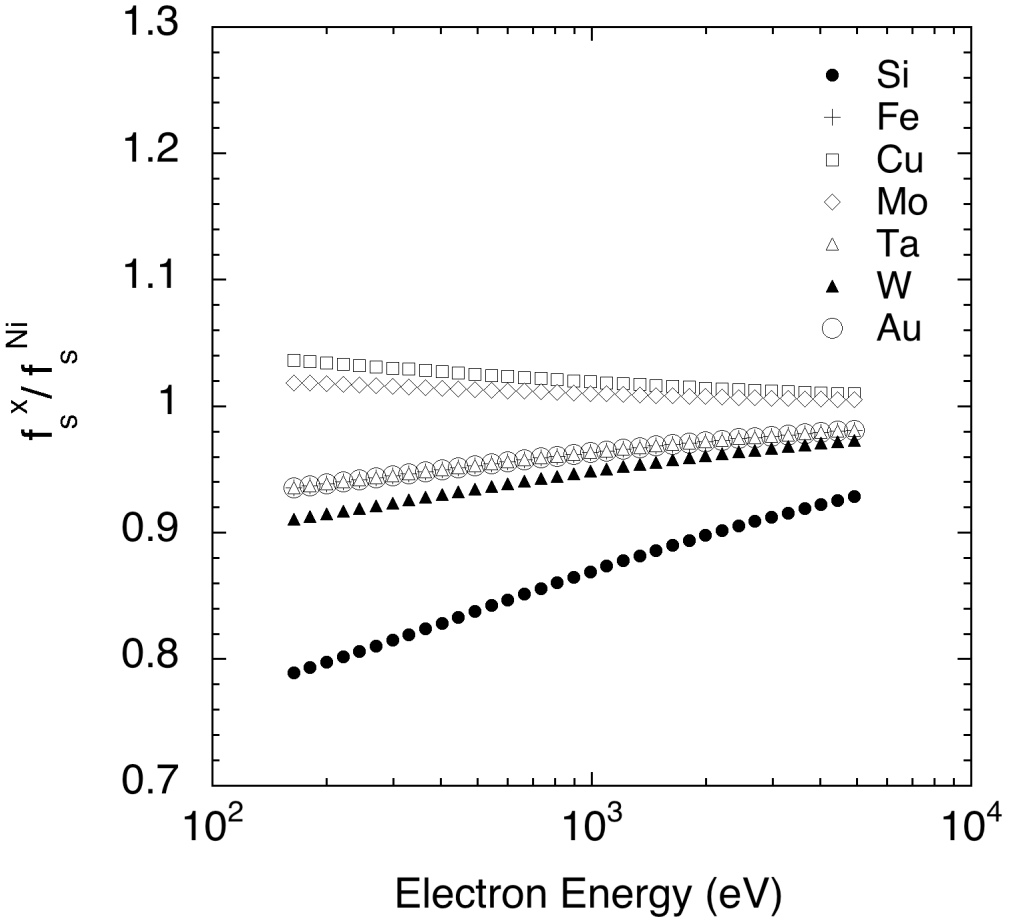
1.3
1.2
1.1
1
0.9
0.8
0.7
10^2
10^3
10^4
Electron Energy (eV)
f_s^x / f_s^{Ni}
Si
Fe
Cu
Mo
Ta
W
Au

Fig. 20

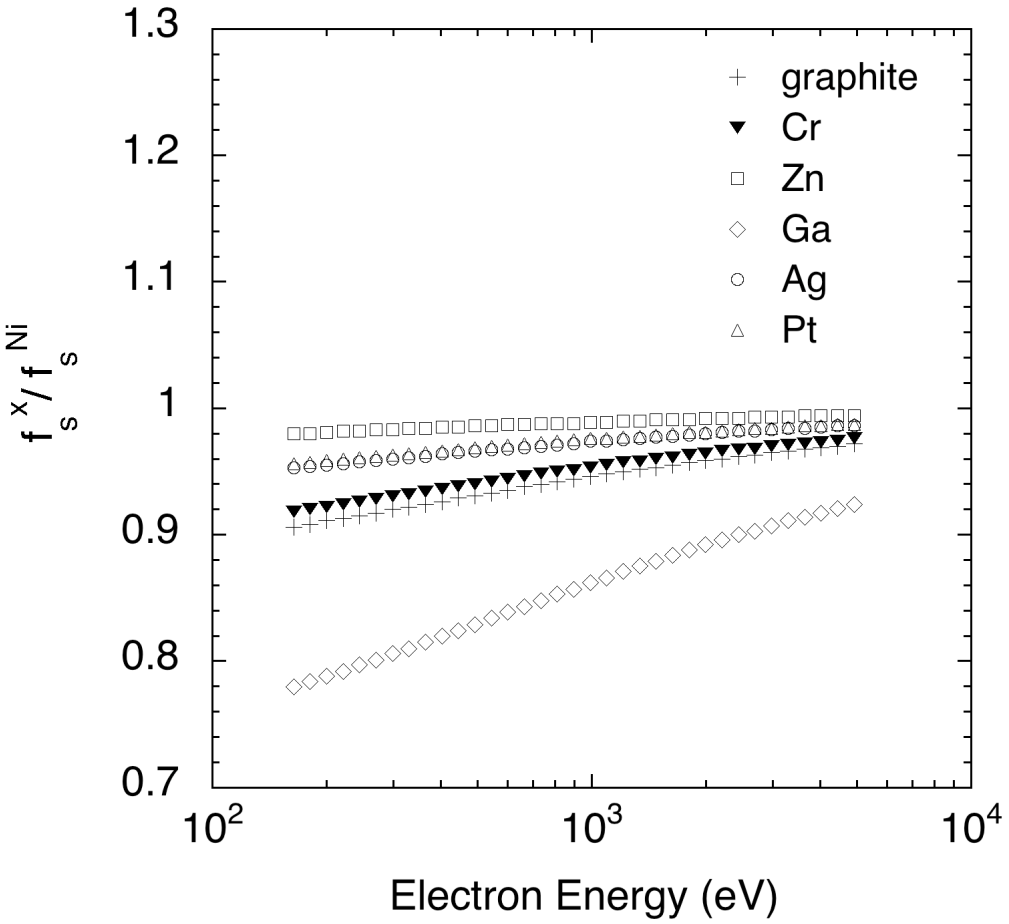
1.3
1.2
1.1
1
0.9
0.8
0.7
10^2
10^3
10^4
Electron Energy (eV)
f_s^x / f_s^{Ni}
graphite
Cr
Zn
Ga
Ag
Pt

Fig. 21

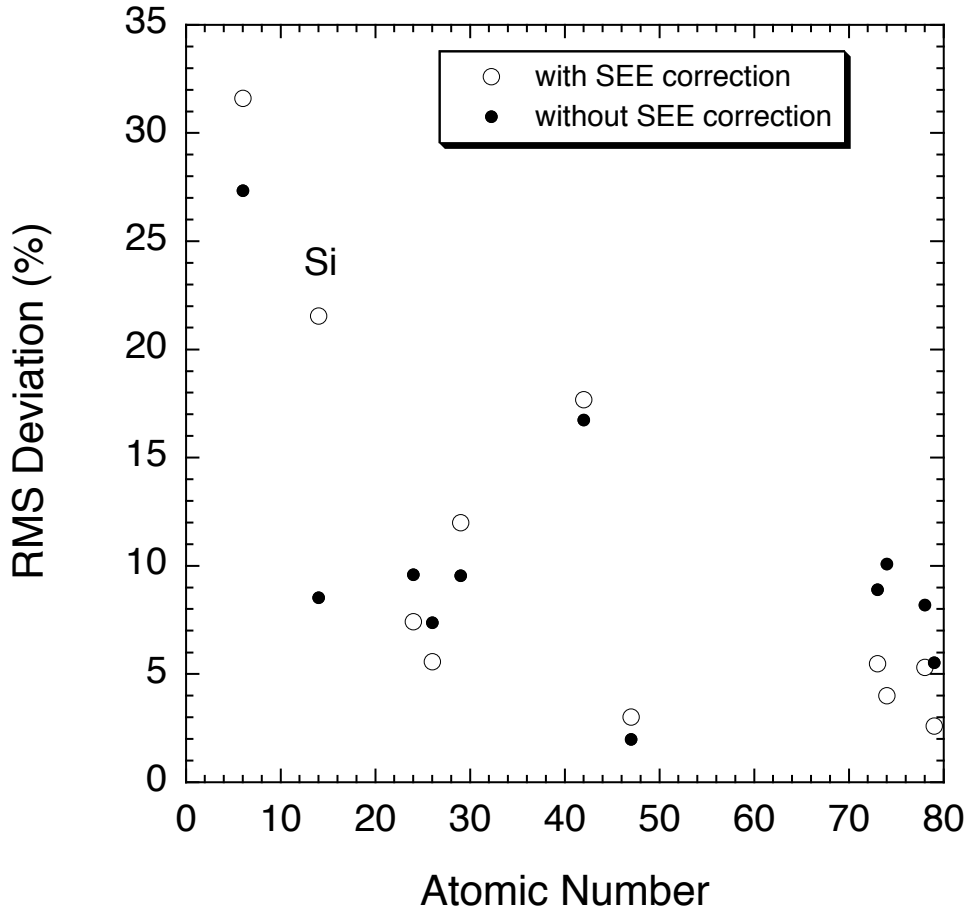
with SEE correction
without SEE correction
Si
RMS Deviation (%)
Atomic Number
0
5
10
15
20
25
30
35
0
10
20
30
40
50
60
70
80

Fig. 22

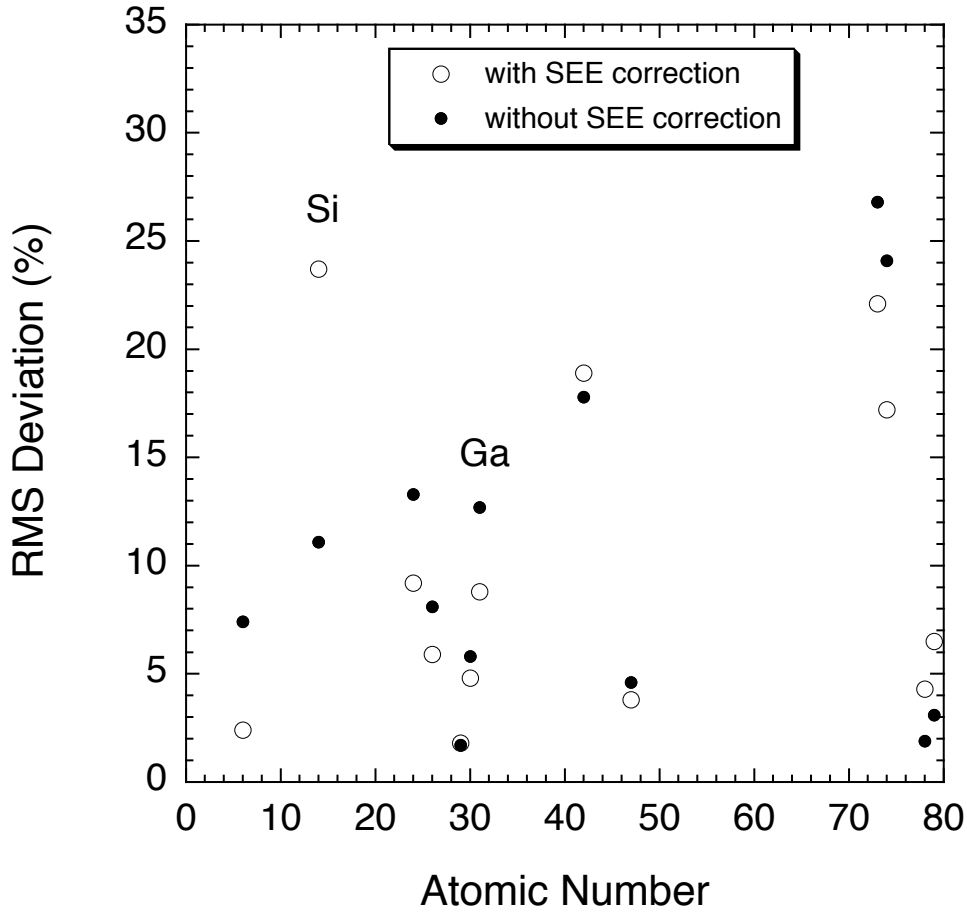
with SEE correction
without SEE correction
Si
Ga
RMS Deviation (%)
Atomic Number
0
5
10
15
20
25
30
35
0
10
20
30
40
50
60
70
80

Fig. 23

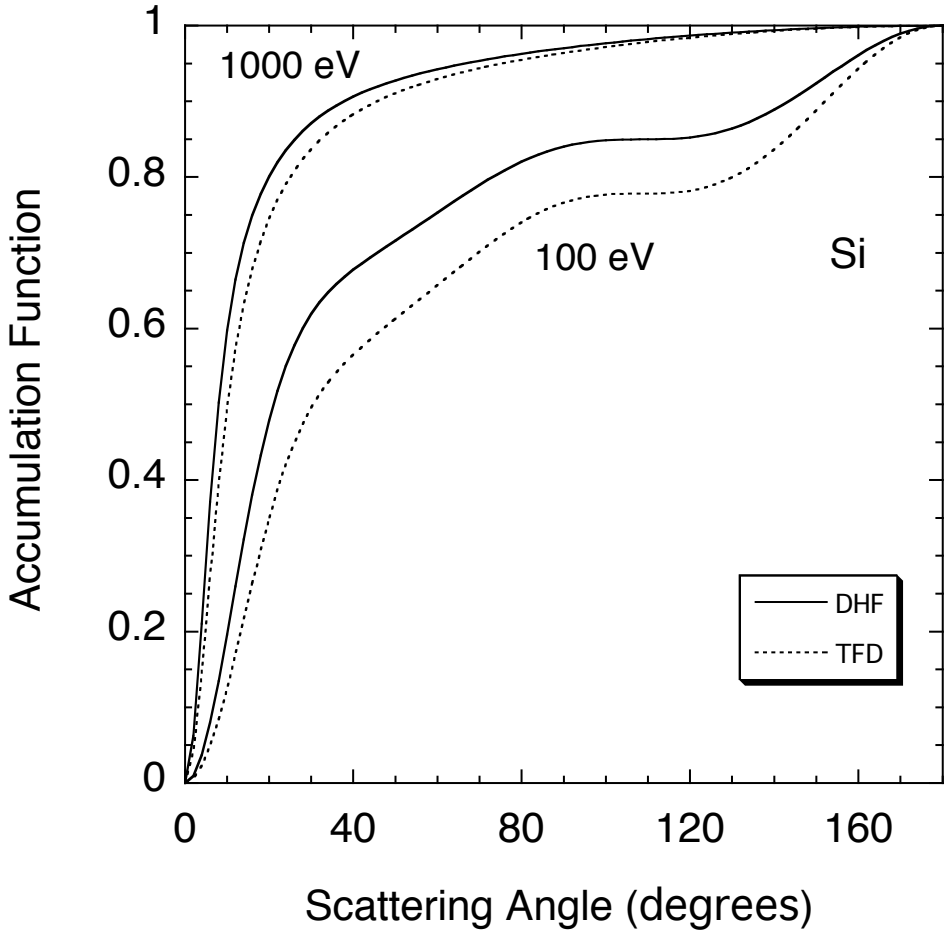
1000 eV
100 eV
Si
DHF
TFD
Accumulation Function
Scattering Angle (degrees)
0
0.2
0.4
0.6
0.8
1
0
40
80
120
160

Fig. 24

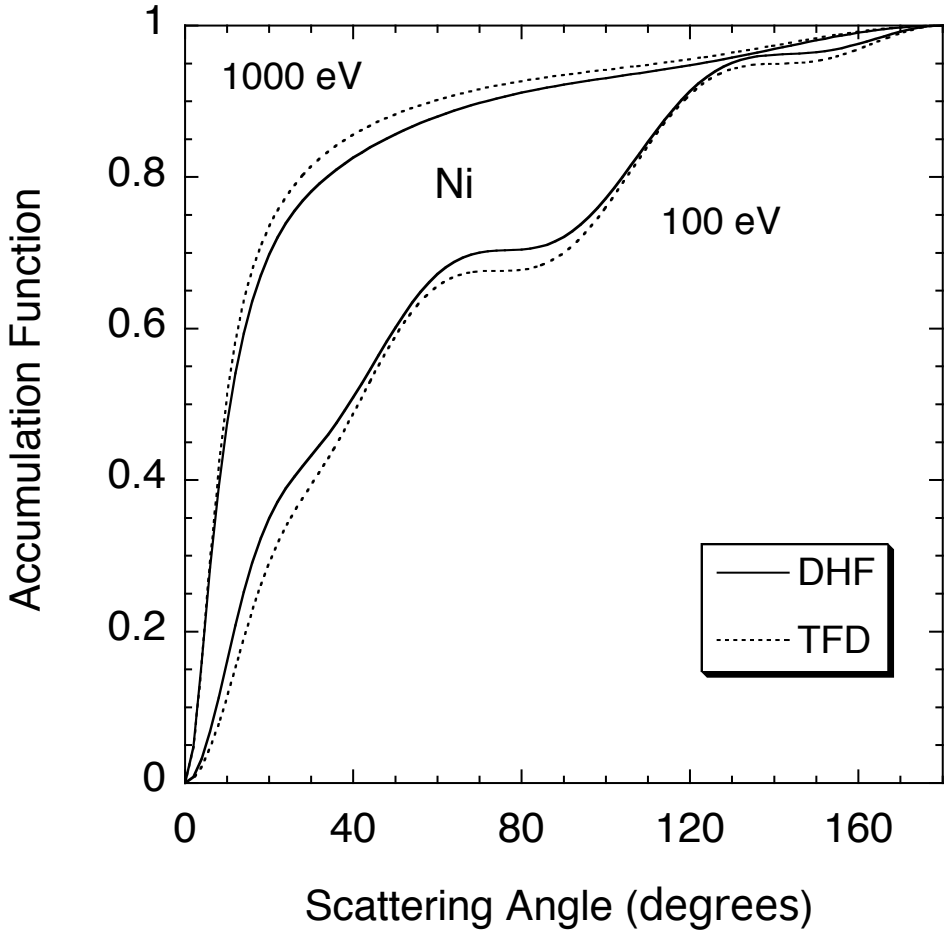
1000 eV
Ni
100 eV
DHF
TFD
Accumulation Function
Scattering Angle (degrees)
0
0.2
0.4
0.6
0.8
1
0
40
80
120
160

Fig. 25

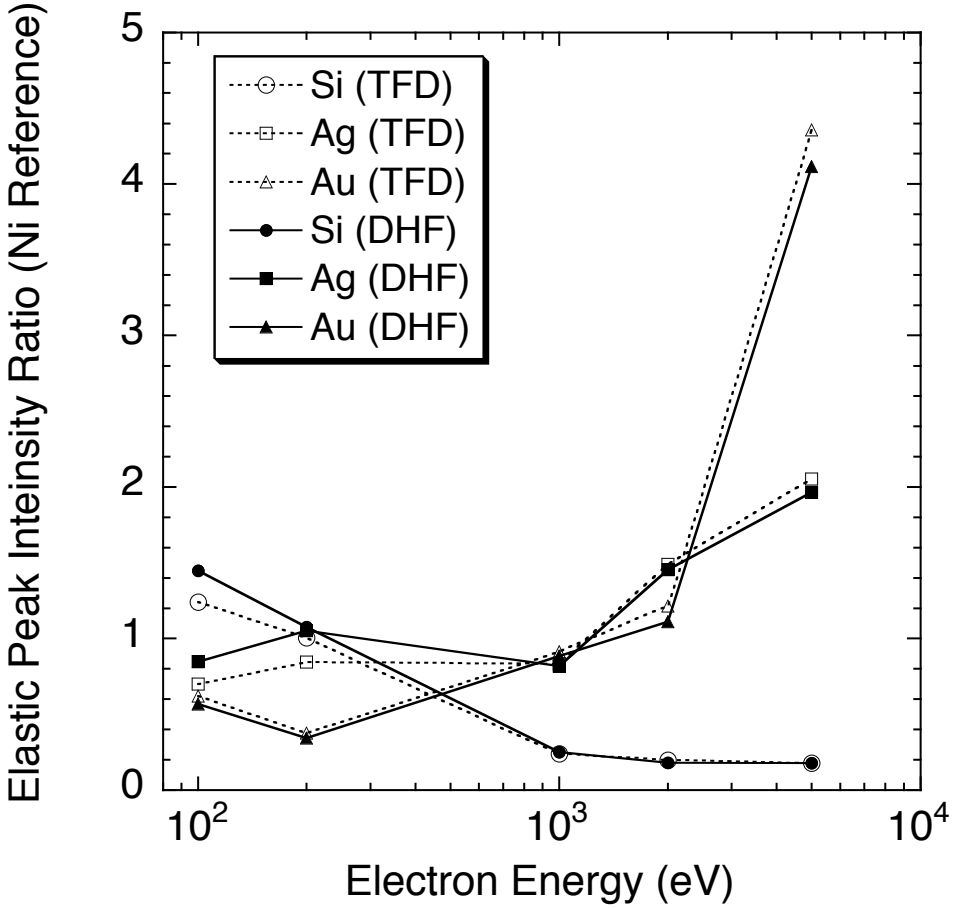
Elastic Peak Inteinsity Ratio (Ni Reference)
Electron Energy (eV)
Si (TFD)
Ag (TFD)
Au (TFD)
Si (DHF)
Ag (DHF)
Au (DHF)
0
1
2
3
4
5
10^2
10^3
10^4

Fig. 26

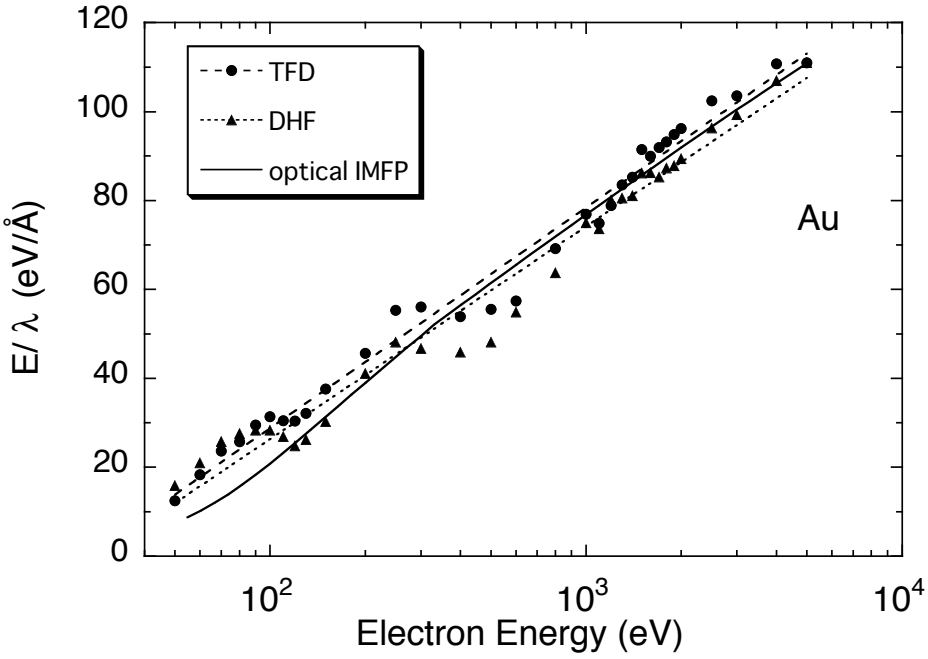
120
100
80
60
40
20
0
E/ λ (eV/Å)
TFD
DHF
optical IMFP
Au
10^2
10^3
10^4
Electron Energy (eV)

Fig.27